Master Thesis in Geographical Information Science nr 215

Detecting Spatial Impacts of Violence through Remote Sensing: A Case Study of Conflict-Affected Regions in Central Mali

Author: J.C.W. van Diest

2026

Department of Earth and Environmental Sciences

Centre for Geographical Information Systems

Lund University
Sölvegatan 12
S-223 62 Lund
Sweden

J.C.W. van Diest (2026). Detecting Spatial Impacts of Violence through Remote Sensing: A Case Study of Conflict-Affected Regions in Central Mali

Master degree thesis, 30 credits in Master in Geographical Information Science

Department of Earth and Environmental Sciences, Lund University

Detecting Spatial Impacts of Violence through Remote Sensing: A Case Study of Conflict-Affected Regions in Central Mali

---

JCW van Diest

Master thesis, 30 credits, in Geographical Information Sciences

Supervisor: David E. Tenenbaum

Department of Earth and Environmental Sciences,

Lund University

Supervisor: Berjo Rijnders

Tilburg School of Humanities and Digital Sciences,

Tilburg University

Abstract

This study investigates if socio-economic indicators can reliably be derived from remotely sensed data and can serve as proxies for detecting and monitoring the spatial impacts of the violent conflict in the Mopti region of Mali. Traditional conflict event databases - like the Armed Conflict Location & Event Data Project (ACLED) – provide point-based event data but often fail to capture gradual spatial shifts that occur when insurgent groups like Jama'at Nusrat al-Islam wal-Muslimin (JNIM) gain territorial control. This study addresses this gap by integrating geospatial intelligence (GEOINT) using remote sensing to track changes in cropland activity, night-time light emissions and changes in built-up area in the Mopti region between 2016 and 2023.

The methodology in this study consists of a multi-indicator approach in which natural environmental variability like seasonal rainfall is filtered out. This was done to ensure that the observed changes can be attributed to the conflict dynamics. Agricultural activity was analysed using the 3-Period TimeScan (3PTS) method, which uses Sentinel-2 NDVI data to visualize the agricultural cycle and makes it possible to identify land abandonment. Population displacements and economic stability were assessed through built-up area growth by using Impact Observatory's Land Classification Land Use (LCLU) deep learning AI algorithms and NASA's Black Marble night-time light radiance values. Different statistical methods were used to evaluate the relationship between these indicators and recorded conflict events in the ACLED event database.

The results of this study suggest that cropland activity serves as a useful indicator of violence-related spatial change, as demonstrated by the identification of villages like Bobosso and Doukoro. In these villages significant agricultural abandonment was directly linked to violent actions by insurgency actors. While a two-way fixed effects model indicated a correlation between night-time light fluctuations and conflict frequencies, this is caused by structural overfitting due to the fixed effect dummies. The variations in night-time light also suggest a broader institutional grid instability due to maintenance issues and fuel shortages. While horizontal urban built-up area growth is evident within the study areas cities and timeframe, a predictive relationship between IDP numbers and built-up area growth could not be established in statistically significant terms. Qualitative research confirmed that an influx of displaced persons does not immediately contribute to an expanded built-up area footprint. IDPs initially find shelter with friends or family or in other communal existing structures.

Keywords: Geography, GIS, Geographical Information Systems, Remote Sensing, Conflict, Mali

Supervisors: **David Tenenbaum & Berjo Rijnders**
Master degree project 30 credits in Geographical Information Science, 2026
Department of Earth and Environmental Sciences, Lund University
Thesis nr 215

Acknowledgements

The human perspective of time is that it is linear. We perceive time as an arrow that moves in one direction from the past, the present to the future. This year in August I will turn 50 and I am fortunate to reach this milestone surrounded by supportive friends and family.

The last four years I spent a lot of time studying. After acquiring a bachelor's degree in Geo Business Intelligence in just 1.5 years' time, I started with the Master Degree in Geographical Information Science at Lund University in January 2024. Now, two years later, as I submit this thesis, it feels as though time has passed in the blink of an eye.

My interest in GIS was sparked at the beginning of the COVID-19 pandemic, when I was asked to implement a GIS portal to track the development of geographic clusters of outbreaks to assist in resource allocation. I really wanted to learn more about the possibilities of GIS, which eventually brought me back to university.

While I am grateful for this opportunity, looking back, I underestimated the weight this journey would place on my family life. I often found myself at a crossroad, choosing between my children's sports events and course assignments. Whether I made the 'right' decisions remains a difficult question to answer. However, the most vital lesson I have learned from the past four years is that time is a scarce commodity for us as human beings.

I want to thank Professor David Tenenbaum from Lund University and Berjo Rijnders from Tilburg University for being my supervisors and the Centre for Information Resilience and the World Food Programme for allowing me to use their pictures.

To Marloes, Carsten and Carice: thank you for your understanding and support. You are, and always will be, what matters most.

Johannes C.W. van Diest

Table of contents

Lists of Figures, Tables and Equations

List of Figures

List of Tables

List of Equations

List of Abbreviations

Abbreviation	Description
3PTS	3-Period TimeScan
ACLED	The Armed Conflict Location & Event Data Project
AFISMA	African-led International Support Mission to Mali
ARIMA	Autoregressive Integrated Moving Average
BRDF	Bidirectional Reflectance Distribution Function
CIR	The Centre for Information Resilience
COIN	Counter-insurgency
EDM	Énergie du Mali
ESA	European Space Agency
FAMa	Forces Armées Maliennes
FAO	Food and Agriculture Organization of the United Nations
GEE	Google Earth Engine
GEOINT	Geospatial Intelligence
HDX	Humanitarian Data Exchange
IDP	Internally Displaced Person
IOM	the International Organization for Migration
JNIM	Jama'at Nusrat al-Islam wal-Muslimin
LAADS	The Level-1 and Atmosphere Archive & Distribution System
LCLU	Land Classification Land Use
MINUSMA	Multidimensional Integrated Stabilisation Mission in Mali
MNLA	Mouvement National pour la Libération de l'Azawad
MODIS	MODerate resolution Imaging Spectroradiometer
NASA	National Aeronautics and Space Administration
NDVI	Normalized Difference Vegetation Index
OLS	Ordinary Least Squares
OSINT	Open-Source Intelligence
RSS	Residual Sum of Squares

Abbreviation	Description
TOA	Top-of-Atmosphere
UCDP	Uppsala Conflict Data Program
UTM	Universal Transverse Mercator

1. Introduction

In the 13th century, the Malian Empire was a powerful west African empire that was well known for its wealth and trade routes, but it gradually declined due to internal and external pressures before coming under French colonial rule at the end of the 19th century (Roberto et al., 2013). French rule and post-independence instability shaped the country's fragile environment, resulting in recurring governance changes and regional disparities that fuel today's conflicts (Roberto et al., 2013).

In 2017 several militant groups merged to form Jama'at Nusrat al-Islam wal-Muslimin (JNIM), which is now one of the dominant jihadist groups in the Sahel (Nsaibia et al., 2023, Provoost, 2019). JNIM aims to establish an Islamic state under Sharia law and is expanding its territorial grip across central Mali by frequently employing violent tactics and intimidation (Nsaibia et al., 2023).

The Mopti region has become a primary area of interest for JNIM's rapid expansion since 2017. This region is uniquely shaped by the seasonal flooding of the Niger River, creating a delicate ecological and economic balance farming and herding communities (Ng'ang'a et al., 2013). However, population growth, environmental stressors and weakening governance have severely disrupted traditional resource-sharing mechanisms between Dogon farmers and Fulani herders (Baba, 2023; Krätli, 2021). Combined with the expansion of violent insurgent groups, these factors have culminated in an intensified humanitarian crises marked by extreme food insecurity and mass displacements (Crisis Group, 2020).

While traditional conflict databases like the Armed Conflict Location & Event Data Project (ACLED) record discrete, point-based events of political violence, they often fail to map the gradual shifts and territorial consolidation that occur when insurgent groups gain control (ACLED, 2023). Remote sensing and geospatial intelligence (GEOINT) introduce critical methodologies to monitor these progressive spatial transitions. This can be done by linking physical and socio-economic indicators like agricultural activity, development in built-up area and night-time lights to conflict dynamics (Zhang & Li, 2025).

This study investigates how indicators like these can reveal violence related spatial dynamics in the Mopti region between 2017 and 2023. By combining contextual socio-environmental knowledge with remote sensing analysis, this research aims to enhance GEOINT methodologies and contribute to understanding of both humanitarian and security oriented aspects in conflict affected regions. The core advancement of this research lies in shifting the analytical focus away from isolated violent events, instead analysing long-term continuous spatial-temporal trends to uncover the broader structural changes driven by territorial presence of insurgents like JNIM's (Nsaibia et al., 2023; Zhang & Li, 2025).

Existing approaches within conflict geography often overlook the subtle, long-term land-use change that is accompanied by territorial consolidation (Krampe et al., 2024; Yin et al., 2019). To address this critical gap, this study evaluates whether remotely sensed indicators can serve as proxies for the spatial development of conflict (Deininger et al., 2024; Xu et al., 2025). By integrating these indicators with localized conflict event data, this research contributes to the growing field of Geospatial Intelligence (GEOINT) (Avtar et al., 2020). Ultimately, this approach enhances evidence-based decision-making within both humanitarian assistance and counter-insurgency (COIN) contexts (Avtar et al., 2020).

2. Aims and Objectives

2.1 Aims, Objectives and Research Questions

The aim of this study is to evaluate whether remotely sensed socio-economic indicators can be reliably used as identifiers of violence-related spatial change in Central Mali. The study also aims to account for and filter out natural environmental variability, including seasonal and interannual differences in rainfall, temperature, and other ecological conditions, to ensure observed changes are attributable to conflict impacts.

The achieve this central aim, the research is structured around following four sequential objectives:

1) Select and derive spatiotemporal indicators of change in cropland activity, settlement size and night-time light emissions from remote sensing and open-source geospatial data sources.
2) Evaluate how effectively these spatiotemporal indicators reflect violence-related spatial changes, while accounting for natural environmental variability (e.g., seasonal rainfall, temperature).
3) Examine how these indicators evolve over time and whether they reveal spatial clusters or hotspots of conflict-related effects.
4) Create a structured workflow for collecting, processing, analysing, and visualizing spatiotemporal indicators to map violence-related spatial change in Central Mali.

The aim and objectives translate into the following central research question and sub-questions that guide the analytical framework:

> *To what extent can spatiotemporal changes in cropland activity, night-time lights emissions and changes in built-up area size changes detected through remote sensing and open-source geospatial data reveal violence-related spatial dynamics in Central Mali between 2017–2023?*

Relevant sub-questions are:

1) *Can a detected change in the cropland activity over time be used as a reliable spatiotemporal indicator of violence-related spatial change in Central Mali?*
2) *Can a detected change in built-up area size over time be used as a reliable spatiotemporal indicator of violence-related spatial change in Central Mali?*
3) *Can a detected change in the night-time light emissions over time be used as a reliable spatiotemporal indicator of violence-related spatial change in Central Mali?*

2.2 Conceptual definitions and operationalization

To establish a measurable baseline for answering the research questions, the key concepts and parameters are conceptually defined and operationalized in this paragraph. This by also linking them to the research field of remote sensing.

2.2.1 Cropland Abandonment

The concept of cropland abandonment is defined as the complete discontinuation of agricultural activities (Weldegebriel et al., 2024). These activities includes ploughing, planting and harvesting of crops on a plot of land during the cropping season.

In semi-arid conflict zones, cropland abandonment typically exhibits a higher overall greenness, because the annual seasonal phenology completely changes (Weldegebriel et al., 2024). The spectral signature can be broken down in two distinct phases:

- Under cultivation: a highly managed seasonal cycle is visible. This is characterized by a distinctive bare soil signature during land preparation and a rapid uniform growth and “greening” during active crop growth and after harvest a sudden drop back to a minimal vegetative signal level.
- Upon abandonment: When human management stops due to conflict induced abandonment, the field undergoes secondary ecological succession (Hishe et al., 2024). In the first 1 to 3 years aggressive wild grasses and perennial weeds take over, after that there will be more and more woody shrubs. As the abandoned fields are left unmanaged wild species will continuously grow, resulting in an increase in total biomass and vegetive density (Weldegebriel et al., 2024). This results into an permanent and constant elevation of measurable “greenness” during the agricultural cycle from start to late summer and autumn compered to maintained and harvested fields, that show a clear pattern in NDVI values indicating managed cropland activity.

Using remote sensing methodologies, abandonment is operationalized by analysing land-use using satellite derived vegetation index, specifically the Normalized Difference Vegetation Index (NDVI). Croplands will be distinguished from natural vegetation based on the greenness (NDVI) values during crop growing cycle from land preparation to harvest.

2.2.2 Internally Displaced Persons (IDPs) effects on built-up area

Internally displaced persons (IDPs) are civilians that are forced away from their homes due to active violence and human rights violations. Unlike refuges who cross international borders, internally displaced persons stay within the country’s borders. Most IDPs move toward nearby regional hubs/cities that they consider to be safe(r) zones. This results in an increased pressure on the already scarce resources in those areas and results in land-use changes, like the expansion of built-up area to accommodate for the influx of people.

Human migration flows themselves are invisible to satellite sensors. Their physical and structural footprint can however be mapped and quantified (Hishe et al., 2024; Weldegebriel et al., 2024). To overcome tracking limitations in conflict zones that are not accessible due to the security situation, this study aims to quantify population displacement by combining IDP numbers with satellite based observation of built-up area development by:

- Applying administrative data on IDP numbers provided by Humanitarian Data Exchange (HDX). HDX tracks IDP number over time, with frequent updates every one to three months. Providing critical ground-truth data necessary for validation.
- Providing a proxy indicator: When thousands of IDPs move to the cities for safety, it creates an immediate demand for shelters. This accelerates the expansion of the cities footprint. By monitoring the growth of the built-up area and check if there is a

Granger causality with IDP numbers, it can be determined if a rise in IDP numbers offers a predictive signal for built-up area growth.

2.2.3 Night-time Light (NTL) Dynamics

Night-time light (NTL) sensors can provide metrics such as the VIIRS data, that can be used to monitor changes and anomalous fluctuations in the night-time light emissions (He et al., 2023). A growing population and change in population behaviour due to violence, will have an effect on night-time light emissions. By monitoring these emissions within the cities footprint and analysing weather there is a predicative relationship with violence against civilians, it can be determined if a rise in violence offers a statistical significant predictive signal for the development of night-time light emissions. This by applying a two-way fixed effects model, providing compensation for fixed effects like differences between cities.

2.2.4 Violence Against Civilians

Violence against civilians consists of deliberate, non-accidental attacks targeted a non-combatants. It is designed to terrorize, control of forcefully remove populations for a specific area. Based on the Armed Conflict Location & Event Data Project (ACLED) database, this study quantifies violence by visualising the individual events as geolocated point data on a map, making it possible to perform geospatial analysis like for example proximity to major roads. All events are presented with their attributes including date, actors, source and number of fatalities to provide useful information on the context and details.

2.3 Hypothesis development and causal mechanisms

Building upon these operationalized definitions, in this paragraph the theoretical mechanisms and econometric models used to test the relationships between civilian violence and spatial change are defined into three to be tested hypotheses.

2.3.1 Hypothesis 1: Violence against civilians and cropland abandonment

- $H1_0$: Using our study data, a logistic regression model of cropland activity and violence against civilians will not yield a significant z-score ($z \leq 1.96$), indicating that violence against civilians does not significantly predict changes in agricultural land use or abandonment.
- $H1_A$: Using our study data, a logistic regression model of cropland activity and violence against civilians will yield a significant z-score ($z > 1.96$), indicating that violence against

Underlying mechanisms

Insurgent violence against civilian populations destabilizes regular activities within communities and triggers responses and coping mechanisms. This also affects agricultural landuse which output is needed to feed local populations. In life and death situations people in farming communities can be forced to flee from their homes and leave agricultural fields unmanaged. In these situations agricultural field where fields are abandoned, these fields rapidly undergo secondary ecological succession. Another effect of the threat of violence is that those who stay, only work the fields that are closest to the villages, leaving the fields that are farthest away from the villages unmanaged. This can also happen due to road blocks, that may also restrict access markets and results in shortages of good like fuel, seeds and fertilizers. Targeted attacks can also result in destruction / burning of crop fields and theft of cattle that is essential to the local farmers, may reduce capabilities to work the fields.

This causal relationship linking insurgent violence against civilians to structural cropland abandonment is thoroughly established in conflict and land-use change literature. The dynamics are for example described in the work of Yin et al. (2019), who combined conflict event data with multi-temporal land-use classification during the Chechen Wars. They confirmed that agricultural zones that were subjected to intense violence have a higher probably of long term abandonment. They also found that there is a minimal chance of post-conflict re-cultivation. A parallel can be found in the research by Xu et al. (2025), who utilized phenology based satellite time series to monitor active conflicts. They demonstrated how large scale conflict triggers rapid cropland abandonment by capturing the distinct spectral signatures of unmanaged cropland fields. These studies confirm that targeted civilian violence leaves and enduring footprint on the rural agricultural landscape, by severing agricultural communities from their lands.

2.3.2 Hypothesis 2: IDP influxes and Built-up area development (Urban Expansion)

- $H2_0$: Using our study data, a Granger causality model of internally displaced persons (IDPs) and built-up area development will not yield a statistically significant F-statistic, indicating no predictive relationship between displacement and growth of the cities in the study area in terms of built-up area.
- $H2_A$: Using our study data, a Granger causality model of internally displaced persons (IDPs) and built-up area development will yield a statistically significant F-statistic, indicating a predictive relationship between displacement and growth of the cities in the study area in terms of built-up area.

Underlying mechanisms

The theoretical assumption that internally displaced persons (IDPs) have a predictive effect on urban built-up areas growth (Granger cause) is based on the mechanisms described in conflict theory. The displacement of civil displacement during armed conflicts is non-random. Fleeing populations systematically seek the relative safety of cities that also function as humanitarian aid hubs and where commercial activities like markets can be sustained. This rapid and localized influx of people, generates an immediate and acute demand for shelter, creating informal settlement in at the borders of these cities. This accelerates the growth of build-up areas to accommodate the expanding human footprint. Statistically establishing a relationship using Granger causality implies that historical fluctuations in IDP numbers contain predictive information for expansions of built-up areas. Proposing a clear directional timeline from human conflict induced migration to physical and detectable built-up area land-use changes.

This relationship between conflict induced displacement and accelerated urban growth, is widely established across remote sensing and demographic literature. When conflict destabilizes rural areas, the relative safety or urban centres experience an anomalous expansion that is stronger than can be explained by economic growth. These dynamics are supported by Weldegebriel et al. (2024), who describes the triggers that result in the influx of IDPs towards urban areas. Also using remote sensing time-series data for tracking the changes to these urban areas with growth of built-up area. This approach allows the researchers to cross verify these physical changes against human metrics. As demonstrated by Li et al. (2017), satellite revealed dynamics during civil crises such as built-up expansions are strongly correlated with the spatial distribution of displaced populations. By establishing this predictive, Granger-causal connection the framework moves beyond static correlations, confirming that the physical footprint of the city is dynamically reshaped by the moving geography of conflict-driven migration.

2.3.2 Hypothesis 3: Violence against civilians and night-time light dynamics

- $H3_0$: Using our study data, a two-way-fixed-effects (TWFE) regression model of Night-time lights emissions and violence against civilians will not yield a significant p-value ($p \geq 0.05$), indicating no statistically significant relationship between conflict events and fluctuations in urban light radiance.

- $H3_A$: Using our study data, a two-way-fixed-effects (TWFE) regression model of Night-time lights emissions and violence against civilians will yield a significant p-value ($p < 0.05$), suggesting a non-random relationship between conflict events and changes in light radiance.

Underlying Causal Mechanism

Targeted violence against civilians, forces them to flee the rural areas and seek the relative safety of the regional urban centres. This results into a heavy concentration of both people and activities (like markets and humanitarian aids) in these surroundings. Using a two-way-fixed-effects model the aim in this study is to look what effect violence against civilians has on the night-time light emission, while also compensating for other effects like maintenance issues of fuel shortages.

The integration of Night-time lights (NTL) as an indicator for conflict and socio-economic change is a robust approach with conflict studies. Changes in night-time light emissions serve as a continuous and remote proxy for measuring human activity and economic stability in areas that are in conflict. Witmer and O'Loughlin (2011) link these satellite observations to the security situation. They used normalized DMSP-OLS night-time imagery to track the impacts of regional wars, demonstrating that variations in light intensity serve as a reliable and objective barometer for the duration and reach of conflict-induced instability. This indicator was also validated by Zhang and Li (2025) looking at the central Sahel crisis based on high-resolution VIIRS data. This data revealed that anomalies and declines in night-time light radiance are directly correlated with violent events causing localized infrastructure destruction, population displacement and institutional collapse. Monitoring NTL emission values provides a responsive indicator of human presence and socio-economic resilience in contested environments.

3. Literature review

> *(…) Thank God, I was able to escape, but the conflict affected me a lot because I left Bankass altogether to come and live with my cousin in Bandiagara, so as not to be killed. I lost my home and my plots of millet that we used to cultivate, not only to feed ourselves but also to sell part of it. And worse, my restaurant activities that allowed me to meet all my expenses also came to an end. Otherwise, the restaurant activities could bring in XOF8,000 to XOF10,000 per day (monthly estimate: XOF240,000 to XOF300,000) before this conflict. And it is the same restaurant that allowed me to build the house where I lived in Bankass because when my husband died, we were renting. Currently in Bandiagara, I only sell rice at noon, and the activity does not bring me much money because here I am not known and the market is not as profitable as in Bankass. Few people buy rice outside. But I find that even at the price of soap, my current earnings are between XOF1,500 and XOF2,500 per day (displaced person in Bandiagara September 2021).*

This testimony is a passage from the article: "*The effects of armed conflicts on local economic dynamics in the Mopti and Ségou regions of Mali"* (Tangara, 2024). It describes how an individual is affected by the violent conflict, resulting in a situation where this person is displaced, suffers a loss of livelihood, and faces instability.

In this case, several levels of Maslow's hierarchy of needs (1943) are adversely affected. A more detailed examination of these human needs -and their relevance to the hypothesis developed for this thesis- will follow in Section 3.3 of this chapter. Before addressing this conceptual framework, Section 3.1 provides an overview of the historical developments and key events that have contributed to the current conflict, while Section 3.2 narrows the focus to the specific study area on which this thesis is based.

3.1 From Empire to Insurgency: The Structural Roots of Mali's Contemporary Conflict

As introduced in Chapter 1, Mali's history has been shaped by political changes and social transformations over centuries. The Mali Empire - established in 1235 - grew into a powerful West African state, known for its wealth and cultural achievements, but it gradually declined by the 14th century due to internal conflicts and external pressures (Roberto et al., 2013).

During the 19th century the French colonization brought Mali under French Sudan, suppressing uprisings and redrawing borders in a way that disrupted local ethnic groups, with the Tuareg in the north as an important example. In the 1950s, the route to independence gained momentum, leading to full independence of Mali in 1960. Modibo Keïta became president and established a one-party socialist government.

In 1968 Moussa Traoré seized power through a military coup. His authoritarian rule resulted in decades of economic difficulties and widespread public discontent. An uprising in 1991 ended Traoré's rule and led to the establishment of a multi-party democracy with elections in 1992 and 1997 (Roberto et al., 2013).

In 2012, Mali experienced a serious resurgence of instability. A Tuareg rebel group named The National Movement for the Liberation of Azawad (MNLA) launched an armed rebellion in the north, mainly around the town of Ménaka (Chauzal & van Damme, 2015). Compared to earlier uprisings, this movement was better organized and equipped, mainly due to weapons from Libya that were sourced after Gaddafi's fall. While the MNLA's initial goal was to establish a greater autonomy in the northern region known as Azawad, they soon established a relationship with Islamist groups such as Ansar Dine, that was being led by Iyad ag Ghali (Provoost, 2019).

The Malian armed forces (FAMa) struggled to respond effectively, which contributed to a coup against President Amadou Toumani Touré and his removal from power. This breakdown of central authority allowed both Tuareg separatist and jihadist groups to take control in the north. Driven by ethnic, political and ideological division, the conflict soon became more complex. It exposed deep-seated tensions between northern and southern communities and historical grievances against the central government in Bamako and the influence of external actors (International Crisis Group (2020).

In 2013, French forces intervened militarily to help the government to regain control over the northern regions. Due to the escalating crises, the United Nations (UN) established the United Nations Multidimensional Integrated Stabilization Mission in Mali (MINUSMA) in April 2013 through Security Council Resolution 2100. MINUSMA was tasked to support the political process helping to stabilize the country, protect the civilian population, and promote human rights (United Nations, 2013). Officially their mission began on the 1st of July 2013, taking over from the African-led International Support Mission in Mali (AFISMA).

In March 2017 Jama'at Nusrat al-Islam wal-Muslimin (JNIM) was formed as Al-Qaeda's Sahelian branch, by a merger of several pre-existing militant groups (Nsaibia et al., 2023). Provoost (2019) provides a composition of these different groups within JNIM, as shown in Figure 1.

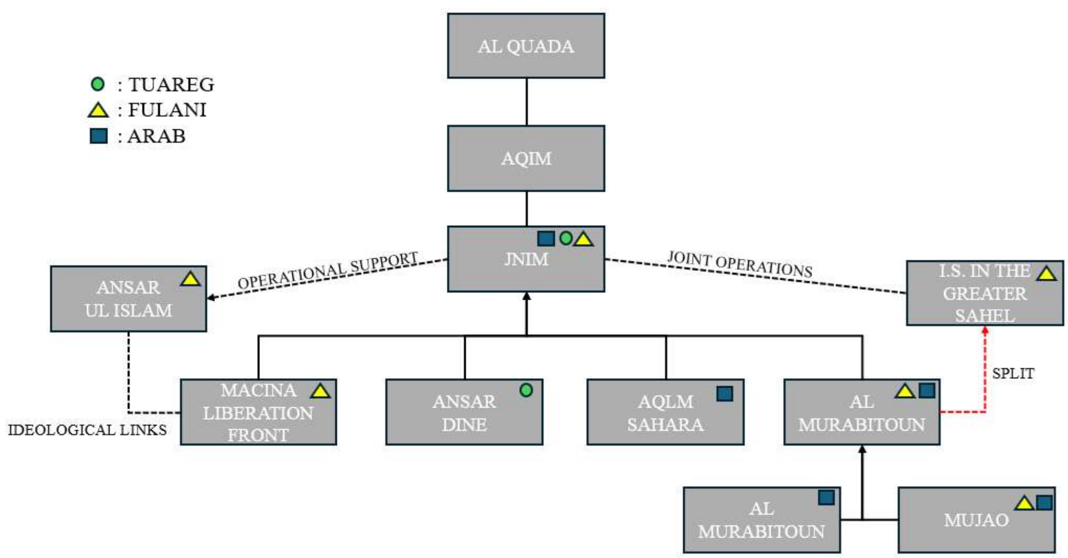

Figure 1: JNIM's composition and links.

The aim of JNIM (Nsaibia et al., 2023) is to establish an Islamic state that is governed by Sharia law in regions under their control. They apply a wide range of methods to obtain control over new regions and do not shy away from using violence.

3.2 Study Area: The Mopti region, Central Mali

The Mopti region, located in central Mali (see Figure 2), covers approximately 67,736 km² and includes the Zone Exondée with Bandiagara, Bankass, Douentza and Koro as the major cities. The region is dominated by the Inner Niger Delta, which is a floodplain of around 16,000 km² that is seasonally inundated by the Niger River, resulting in a landscape of wetlands, dry savannas, and sandy plateaus (Ng'ang'a et al., 2013).

The region was selected for this study due to its agricultural and pastoral zones, its high frequency of conflict incidents and its rich availability of open-source geospatial data. These characteristics make it a representative case for analysing spatial indicators of violence-related change in Mali.

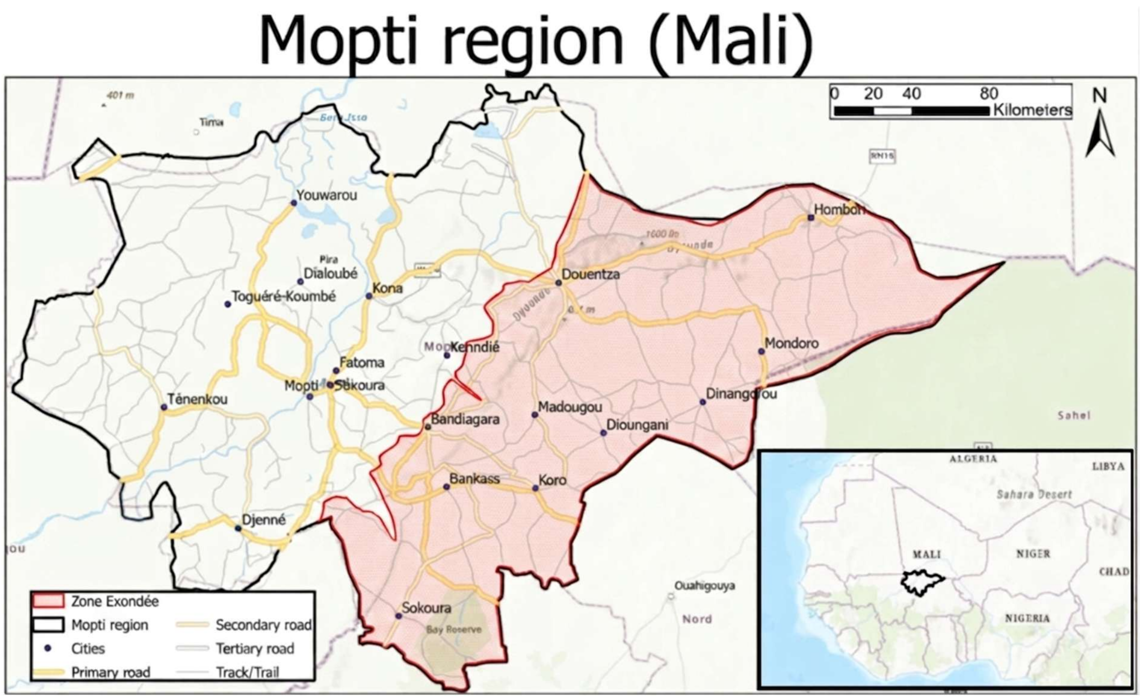

Figure 2: Location of Mopti region within Mali / Western Africa (Source: Based on standard ESRI layers, HDX road layer and Zone Exondée delineation by author)

Agriculture is the backbone of Mopti's economy, with most households engaged in crop farming. Livestock farming is equally important, making the region one of Mali's leading livestock production zones. Mopti accounts for approximately 28% of the national cattle population and 18–19% of sheep and goats (Statafric, 2023 and Baba, 2023), contributing significantly to household income and food security through both transhumant and sedentary herding systems.

The ecological dynamics of the Mopti region are shaped by the Niger and Bani Rivers. Their annual flood cycles create fertile floodplains that support crop cultivation and livestock grazing. The seasonal variations determine the crop planting schedules, grazing routes, and fishery activities (Bonkoungou et al., 2024). Anomalies in the average yearly pattern like reduced or delayed flooding, results in a decrease of available pasture. This increases pressure on herders and potentially resulting in more conflicts about scarce resources.

In the past, Dogon farmers and Fulani herders found a balance and were able to come to arrangements about shared grazing of crop residues and rotation access. The balance has been challenged and disturbed by population growth, intensified agricultural use and declining pasture availability (Krätli, 2021). Weakened traditional institutions, reforms and environmental challenges like erratic rainfall and changing flood patters, have complicated the situation (OECD, 2021). Due to these factors local resource management has become even more complicated, especially with insecurity rising and presence of armed groups (Baba, 2023).

Within the Mopti region, the area historically known as Macina in the east is the area that is dependent on the seasonal Niger river floods. The Zone Exondée, located in the south and east of the region, lies outside this regularly flooded delta and is experiencing the highest increase in communal violence in the region. This violence is induced by the uprising of JNIM and, more specifically, the Macina Liberation Front also known as Katiba Macina. The presence of these groups and minimal state presence has created a highly fragile security environment (Crisis Group, 2020).

The focus in this study is the Zone Exondée, which includes the regions Bandiagara, Koro, Bankass and Douentza, emphasizing their immediate surroundings and the primary access routes connecting them. Chauzal & van Damme (2015) explain that the communities that live in Mali are deeply divided, as discussed in this chapter. They present a map -as shown in Figure 3- where the distribution of different ethnicities in the country is presented. The colours represent the majority in each region. The Mopti region with Zone Exondée is outlined in red.

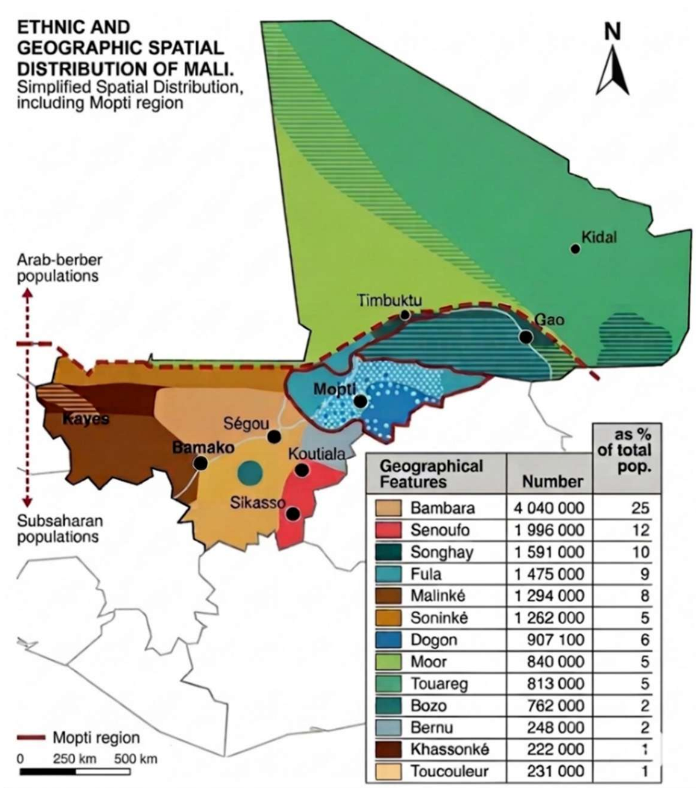

Figure 3: Ethnic groups in Mali (adapted from Chauzal & van Damme, 2015, Map 4)

The historical and environmental drivers of the conflict in Mali are well documented. There, however, remains a methodological gap in linking remote sensed indicators to the conflict dynamics. Most studies have focused on discrete events rather that progressive spatial transitions. This study builds on recent work by Zhang & Li (2025), extending their approach and suggestions for further research to the Mopti region to assess the temporal and spatial correlation between geospatial indicators and conflict activity.

3.3 Complex Adaptive Conflict System

Human behaviour is closely related to the extent to which fundamental needs are met. This both applies to individuals and societies. Maslow's hierarchy of needs conceptualises these needs and arranges them in a gradual order. This includes the basic physiological requirements for safety, as well as social belonging, esteem and ultimately self-actualisation (Maslow, 1943). In insecure environments - like currently in the Mopti region of Mali - even the most basic and essential levels of this hierarchy become difficult to achieve. When such basic core needs as safety, food security or economic stability are undermined, individuals and communities may adopt coping strategies that given the situation, can contribute to a cycle of violence.

Several conflict frameworks help clarify why violence emerges and persists in these situations. The greed–grievance perspective (Collier & Hoeffler, 2004) is an example. It separates the material motivations that make rebellion attractive from the social, political and identity-based grievances that drive collective mobilisation. The human needs theory (Burton, 2024) builds on this by arguing that conflicts intensify when essential needs are denied or are inadequately addressed by institutions, leaving affected groups with only limited peaceful avenues through which to seek redress.

Galtung's concept of structural violence (Galtung, 1969) complements these perspectives by highlighting the deeper social, political, economic and environmental arrangements that systematically restrict people's well-being. These long-term constraints form part of a layered/tiered conflict model comprised of:

- Structural factors
- Trigger events
- Individual or institutional responses
- Observable outcomes

This multi-layered approach captures the dynamics of enduring crises, such as the conflict in Mali, where triggers and responses accumulate over time and produce distinct spatial, social and economic consequences.

Looking back to the period before 2016, the stressors in the Mopti region appeared more isolated from one another. Over the years, these disparate pressures have become increasingly interconnected. They have resulted in an environment in which social, cultural, political, economic and environmental factors continually interact and reinforce each other in conflict.

This reflects what Homer-Dixon (1999) refers to as an example of a complex adaptive system. That is, a system in which small changes can generate unpredictable outcomes and were feedback loops shape behaviour. The conflict adapts as actors and conditions evolve.

Based on these factors and interactions, the following layered conflict model is constructed - see Figure 4- for this study based on the conducted literature study. The model utilizes the food insecurity framework of Insecurity Insight (2024) as a baseline, augmented with further factors to provide a more comprehensive view of the regional crisis.

The layered conflict model in this study is structured into four interconnected tiers. The topmost layer is shown in purple and represents the enabling factors and underlying structural elements (social, cultural, political, economic and environmental) that shape everyday vulnerabilities.

On the left, the conflict events are highlighted in orange. They visualize immediate triggers such as attacks, looting and other violence against civilians that disrupt everyday life and existing systems. The central blue layer captures human and systems responses to these events. These responses include displacement, reduced trade, and various coping strategies adapted by affected communities. At the bottom, the observable outcomes are presented in red, which in this study directly correspond to the proposed hypotheses in Chapter 2.

Summarizing the events that have taken place between 2017 and 2023 in the study area, the five enabling factors did not only get worse individually, but by increasingly reinforcing each other, they resulted in a self-sustaining, reinforcing feedback cycle of instability. The local power vacuum caused communities to rely on ethnic militias or armed groups for security, which increased tensions between Dogon and Fulani communities. At the same time the scarcity of resources and disruption of livelihoods is making communities and individuals increasingly vulnerable and pushes them towards these armed groups or criminal activities. The loss of livelihoods and economic decline further undermines trust in governmental institutions, fuelling support for insurgency actors. As the social and cultural mistrust grow, they also erode the traditional mechanisms for sharing land and water. These interconnected dynamics create reinforcing feedback loops where environmental stress, economic hardship, political instability and social division continuously amplify each other.

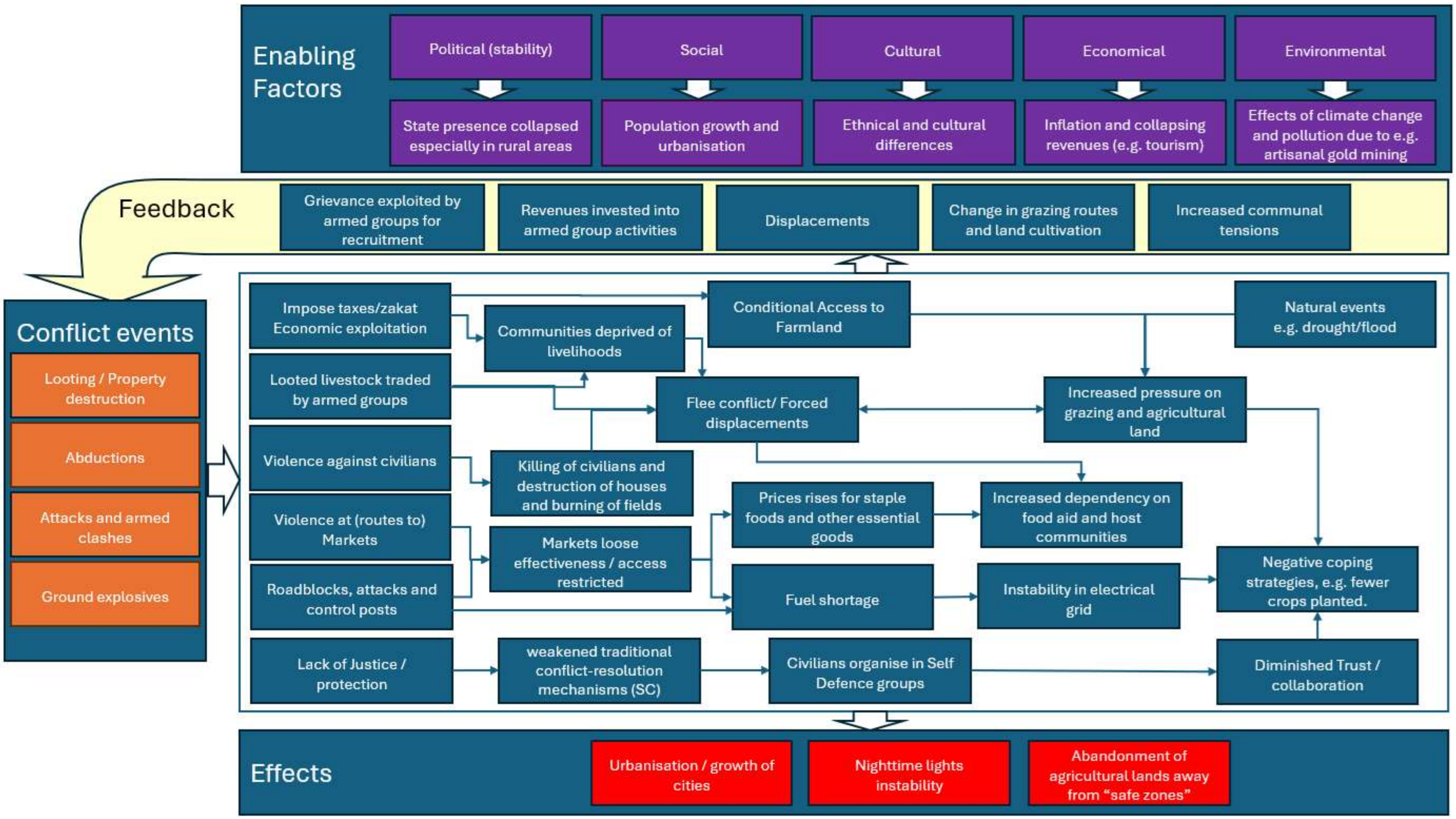

Figure 4: Layered conflict model. Adapted from Insecurity Insight (2024) with additional elements based on literature review

3.4 Conflict remote sensing theory

The field of conflict remote sensing has evolved from localised qualitative damage assessments to a discipline capable of mapping the resulting spatial disruptions. Armed conflicts have a profound effect on human interactions and behaviour, which can result in rapid land-use changes. In regions with active and highly volatile violence, the insecurity situation makes it impossible to perform traditional field research. Remote sensing offers an objective, safe and non-invasive methodology to monitor changes in these areas. By isolating and evaluating specific indicators it becomes possible to distinguish conflict driven spatial impacts from broader environmental variations and background noise.

The explicit relationship between localized violence and empirical land-use alterations has been extensively quantified by Yin et al. (2019). In assessing agricultural abandonment during and after the Chechen Wars, Yin et al. (2019) integrated geospatial conflict event points with multi-temporal satellite classifications. By executing regression models that interacted the distance to conflict events with localized intensity, their findings confirmed that agricultural plots in close proximity to active fighting exhibited a significantly higher probability of long-term abandonment. This pattern mirrors spatial dynamics observed in other conflict zones, such as northeast Syria. There, Eklund et al. (2024) integrated multi-temporal satellite classifications to untangle the complex, overlapping feedback loops where environmental drought, structural economic reorganization and migration interact to drive widespread land abandonment.

Beyond rural landscapes, the spatial footprints of violence fundamentally alter urban configurations. While localized violence typically affects structural urban growth within targeted metropolitan centres, regional safe-haven hubs frequently experience rapid, unplanned expansion driven by sudden influxes of internally displaced persons (IDPs). To capture these dynamics beyond physical built-up footprints, the utilization of night-time lights (NTL) remote sensing has emerged as an invaluable proxy for mapping shifting socio-economic activity and structural civil disruption (Zhang and Li, 2025).

Within active conflict zones, a persistent dimming or total "blackout" of night-time light radiance generally serves as a direct indicator of catastrophic electrical grid failures, widespread urban depopulation, or systemic localized economic collapse. For example, Witmer and O'Loughlin (2011) utilized radiometrically normalized NTL imagery to empirically detect the spatial footprint of conflict across the Caucasus, demonstrating that variations in light intensity offer a highly reliable barometer for evaluating both the intensity and duration of conflict-induced instability.

Li et al. (2017) utilized VIIRS data to track the longitudinal developments of the Syrian Civil War, establishing that fluctuations in night-time light radiance were strongly correlated with both localized IDP numbers and the physical destruction of critical civic infrastructure. This underscores that NTL metrics extend beyond the simple measurement of electrification. They function as multi-dimensional indicators of human presence and social and economic resilience. Consequently, when rural agricultural zones darken in simultaneous synchronization with a measured decline in the Normalized Difference Vegetation Index (NDVI), it yields a powerful cross-validation. This dual signature indicates that both the localized labour force and structural agricultural productivity have been effectively severed by the ongoing conflict.

Ultimately, synthesizing cropland abandonment tracking, urban built-up classifications and night-time light metrics yields a holistic, multi-indicator framework. This integrated approach successfully captures the continuum of conflict impacts across interconnected urban and rural geographies. Empirical studies in Burkina Faso by Kafando and Sakurai (2024) further validate this spatial intersection, demonstrating that militant and terrorist violence significantly suppresses both agricultural productivity and total crop output. These complex landscape degradations can subsequently be mapped and evaluated against the fluid, shifting spatial intensities of urban light emissions and rural vegetation dynamics.

4. Methodology

This chapter outlines the methodological approach used to examine whether remotely sensed indicators can reveal spatial impacts of violence in the study area in Mali between 2017 and 2023. Building on the hypotheses and conflict model introduced in earlier chapters, the methodology explains how conflict data, satellite observations, and auxiliary geospatial information were collected, processed and analysed. The aim is to show clearly how each analytical step contributes to testing the relationships between conflict events and measurable changes in cropland activity, night-time lights and settlement patterns.

The research follows a quantitative, spatial-analytical design, complemented by insights from existing literature. This combination supports a systematic investigation of spatiotemporal patterns of violence while ensuring that the interpretation of geospatial indicators remains grounded in contextual understanding of the conflict environment.

These methodology steps in the study are presented in Figure 5 and described in this chapter.

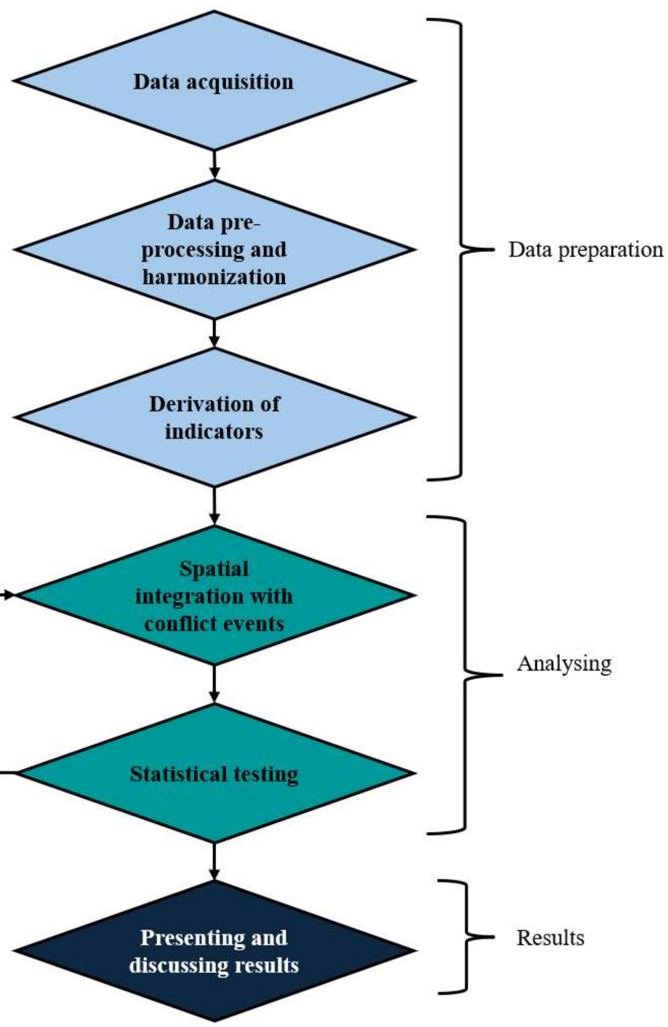

Figure 5: Methodology used in this thesis.

4.1 Research Design

The study applies a quantitative geospatial-statistical workflow, designed to link conflict dynamics to observed change(s) as measured through remotely sensed indicators. This approach is well suited for two reasons.

First, the expansion strategies of armed groups in central Mali often unfold gradually and may not be fully captured by event-based datasets alone. Second, satellite observations allow continuous monitoring enabling the detection of subtle changes that may correspond with shifts in territorial control or human activity.

The analytical framework is built around the following components:

a) Data acquisition from ACLED, Sentinel-2, National Aeronautics and Space Administration (NASA) Black Marble and auxiliary GIS sources.
b) Geospatial processing to select and derive indicators for cropland activity, night-time light emissions and built-up areas.
c) Integration of conflict data with these indicators through spatial joins and zonal statistics.
d) Statistical analyses to assess whether changes in these indicators are effective at indicating conflict activity.

The study area focusses on Mopti's area known as the Zone Exondée, which includes the regions Bandiagara, Koro, Bankass and Douentza. In each of these regions the main city has the same name as the region.

4.2 Data Sources

A combination of conflict data, satellite imagery and contextual GIS layers form the empirical basis of this study. The different datasets used in this study are described in the following paragraphs.

4.2.1 Conflict Event Data

The Armed Conflict Location & Event Data Project (ACLED) is a real-time dataset that records political violence and protest events worldwide. It provides the spatial and temporal distribution of violent incidents. Each event includes coordinates, date, actors involved and event type. These attributes serve as the primary dependent variable when analysing how conflict relates to changes in remote sensing indicators. ACLED (2023) uses a data review and cleaning process to ensure data quality.

The ACLED data for Mali includes events such as cattle theft and the burning of granaries, making it a valuable source for analysing the spatial and temporal patterns of conflict. The data for the study area for the period 2017-2023 is downloaded as CSV file and imported into ArcGIS Pro as vector layer with points data. In total this concerns 2273 recorded events.

The recorded events in the study area from 2017-2023 can be divided in the event types as shown in Table 1.

Table 1: Occurrences of different events in ACLED database in study area 2017-2023

Event Type	Description	Occurrences
Battles	Armed clashes between state or rebel groups	639
Explosion/remote violence	IED's and air drone strikes	320
Protests	Protest from different groups	71
Riot	Violent demonstration	15
Strategic development	Looting, property destruction and disrupted weapons use	319
Violence against civilians	Attacks and abductions	909
Total		**2273**

4.2.2 Remote Sensing Data

Cropland land use / activity

To acquire data on cropland activity global or continental land cover and land use datasets (LCLU), such as the global land cover datasets from the Food and Agriculture Organization of the United Nations (FAO) and the European Space Agency (ESA) were investigated. They are widely used but perform poorly in the Sahel. In this region, agricultural fields are typically small, fragmented and are strongly influenced by seasonal changes, which causes these datasets to provide low accuracy on classifying cropland in the Mopti region. Because of these shortcomings, traditional LCLU datasets are not suitable for detailed, site-level monitoring of cropland in the study area.

The diverse agroecological conditions in the Sahel mean that machine learning approaches need to be highly site-specific to accurately identify cropland. This challenge is compounded by a shortage of suitable training data, as field sampling is limited due to restricted access in the region.

To address this, this study used the 3-Period TimeScan (3PTS) method, which relies on Sentinel-2 satellite imagery to track the seasonal growth of vegetation. The method is developed by Boudinaud (2019) and applied by Boudinaud and Orenstein (2021) in the Mopti region. By dividing the growing season into three periods and capturing their maximum NDVI values (between June 15th and October 15th), this method makes it possible to -visually-distinguish cropland from other vegetation types. This is done by synthesizing the temporal progression of the growing season into a single product. Landsat data was considered, but its 30-meter resolution is too coarse for the small and manually cultivated agricultural fields in the study area.

Sentinel-2 Level-1C imagery (10 m resolution) is used to monitor vegetation dynamics. Its frequent revisit time (5–6 days) makes it suitable for analysing seasonal cropland cycles. On average, 20 images (using bands B4 and B8 to derive NDVI values) for each year during the 2017-2023 period, will be used to monitor the cropland development.

For this study, multispectral imagery from Sentinel-2 was used. Sentinel-2 is a high-resolution, wide-swath Earth observation mission developed by the European Space Agency (ESA) under the Copernicus program, designed to monitor terrestrial and coastal environments. The mission provides data relevant for land cover, vegetation, soil and water monitoring, as well as inland water bodies and coastal zone observations.

The dataset employed in this study corresponds to Level-1C Top-of-Atmosphere (TOA) reflectance products and comprises between 200 and 300 granules collected for each year. Each granule contains 13 spectral bands with a radiometric resolution of 16-bit unsigned integers, with a pixel size of 10 meters. In addition to spectral data, the dataset includes quality assessment (QA) bands, notably QA60, which provides a cloud mask using a bitmask encoding for opaque and cirrus clouds. The analysis is performed using the Google Earth Engine (GEE) and an adapted 3PTS script (Boudinaud, 2019).

The spectral bands used in this study cover the visible, near-infrared, red-edge and shortwave infrared regions (B1–B12), with the primary bands for visualization being the red (B4), green (B3) and blue (B2) bands.

This study analyses year-to-year cropland changes during the 2017-2023 period.

The primary crops cultivated in the study area (Zone Exondée) include millet, sorghum, cowpeas, and groundnuts (Famine Early Warning Systems Network, 2015). These crops are reliant on rainfall and typically have a cultivation cycle ranging for 60 to 100 days from sowing to harvest (June – September). The 3PTS method and data used covers this growing cycle.

In November 2019, field visits were conducted in the Koro, Bankass, and Bandiagara regions by Boudinaud and Orenstein (2021) to gather ground-truth information on cropland changes. Observations included cultivated areas, abandoned fields and damaged infrastructure, complemented by qualitative interviews with residents about the impact of conflict on farming and market access. This field data acquired by Boudinaud & Orenstein (2021) was used to validate satellite-based analysis, confirming patterns of cropland reduction and abandonment identified in remote sensing imagery.

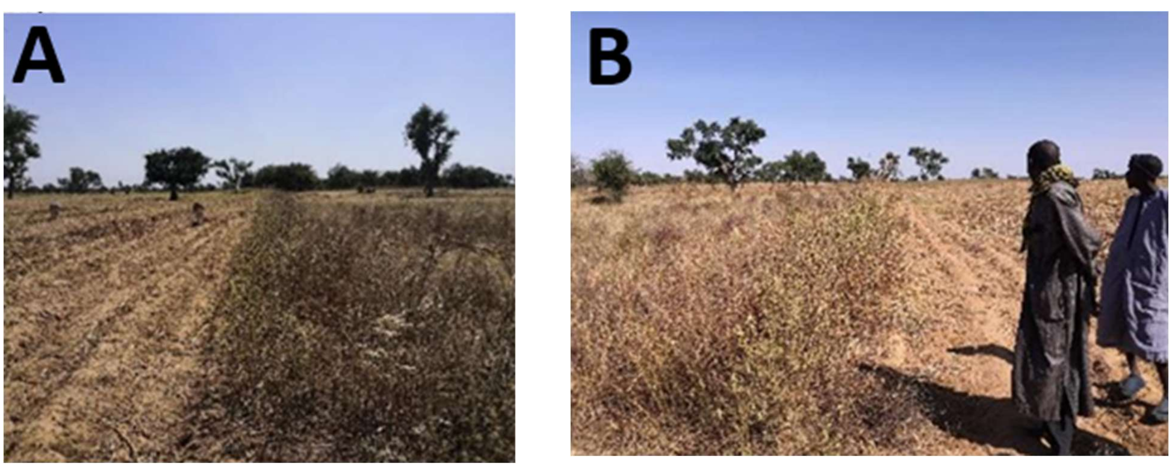

Figure 6A: On the left is shown a cultivated field after harvest, in the surroundings of Birga-Peulth.
Figure 6B: Villagers in Déri showing the neat delineation, beyond which they could not cultivate in 2019.

Using the 3PTS composites land use classes were inferred directly through systematic visual interpretation of these multi-temporal colour signatures, combined with ground-truth reference data and high-resolution spatial baselines. Because traditional automated classifiers frequently struggle with the high seasonal variability and spectrally homogeneous bare soils of the Sahelian landscape, visual analysis of the composite colour trajectories was chosen to ensure contextual accuracy.

Built-up areas

To see the development of the built-up area for rural settlements and cities in the study area, a LCLU classification will be used to determine changes in the built-up areas in the regions of Bandiagara, Koro, Bankass and Douentza.

The LCLU classification used is the 9 class Landcover dataset from Impact Observatory which is available as open access for all years of the study. This time-series dataset will be accessed through the ESRI Living Atlas. It is based on Sentinel-2 Level-2A imagery with a 10-meter resolution. To ensure consistent surface reflectance across the time series, the imagery underwent atmospheric correction via the Sen2Cor algorithm to mitigate aerosol scattering and absorption artifacts. The Algorithms used for the classification are provided by the Impact Observatory's deep learning AI land classification model. The algorithm also uses the spatial context of the surrounding cells to determine the classification of a specific cell. Karra et al. (2021) concluded that model provides an 80% precision (user's accuracy) and 95% recall (producer's accuracy) for built-up areas as stated by Impact Observatory.

Built-up areas are described by Impact Observatory (n.d.) as:*" Human made structures; major road and rail networks; large homogenous impervious surfaces including parking structures, office buildings and residential housing; examples: houses, dense villages / towns / cities, paved roads, asphalt."*

Airbus Pléiades (Neo) imagery -accessed via Google Earth pro- are used as a visual reference for qualitative validation.

Night-time lights

NASA Black Marble VNP46A3 (15 arc seconds resolution) data provides monthly, atmospherically corrected radiance values for analysing night-time lights as a proxy for human activity, economic conditions and settlement stability.

For monitoring the night-time lights, the Black Marble (VNP46/VJ146) data suite will be used, more specifically the VNP46A3. The details of this dataset are described in a user guide (NASA, 2021). This dataset offers a monthly product generated from daily measurements that have been corrected for atmospheric, lunar, and angular effects, with a spatial resolution of 15 arc seconds (roughly 465 meters). Data pre-processing steps included image mosaicking, cropping, elimination of background noise and map projection into the Universal Transverse Mercator (UTM) Zone 30N coordinate system. An all-angle snow-free layer is used.

For each city, cells were selected that are in built-up areas in all years. In the following table show the number of cells for each city.

Table 2: Number of selected cells for analysis in each city

City	Number of cells
Bandiagara	31
Bankass	19
Douentza	28
Koro	17
Djenne	24
Mopti (including Severe)	163

4.2.3 Auxiliary data

To enrich the analysis and support interpretation, additional datasets are used:

- CHIRPS rainfall data (5 km resolution) to contextualize environmental variability;
- Administrative boundaries (Regions);
- Road networks from the Humanitarian Data Exchange (HDX);
- Digital elevation model;
- IDPs from the Humanitarian Data Exchange.

All datasets were selected based on availability, spatial coverage and relevance to the hypotheses.

Table 3: Auxiliary datasets

Dataset	Source	Resolution	Type	Temporal coverage	Purpose
CHIRPS	Climate Hazards Centre	5km	Raster	Monthly 2017-2023	Rainfall patterns, perception in mm
Administrative borders	HDX	Adm. levels 1-3	Vector	2019	Division of administrative regions
Roads	HDX	All roads	Vector	2014	Roads in Mali
DEM	Copernicus	10 Arc Seconds	Raster	2014	Digital Elevation Model
IDPs	HDX	Adm. levels 1-3	Vector	2017-2023 4 to 6 yearly updates	Tracking of Internally Displace Persons in Mali.

4.3 Data Collection and Preparation

Data collection involved acquiring datasets from open-access sources or institutional repositories. All data were cleaned, standardized and georeferenced to ensure spatial compatibility. Missing or inconsistent data were addressed through imputation or exclusion as appropriate. Spatial data were projected into the same coordinate system to enable overlay analysis and variables were aggregated or normalized to facilitate comparison across different spatial and temporal scales.

All geospatial data were standardized to ensure consistency across sources. Steps included:

Projection standardization: All layers were reprojected into Universal Transverse Mercator (UTM) Zone 30N coordinate system to enable overlay operations. As this projection provides low distortions across multiple properties at pertinent scales (conformal projection) and thus enables accurate distance measurements within the zone. Mopti falls within UTM Zone 30N, which spans from 12°W to 6°W longitude.

- Data cleaning: Missing or inconsistent entries were corrected or excluded.
- Spatial alignment: Raster datasets were clipped to the study area and vector data were aligned to city buffers and road networks.

- Temporal structuring: ACLED events and satellite observations were organized into annual and monthly intervals, depending on the indicator being analysed.

This harmonization ensured that variables could be compared reliably across time and space.

4.4 Geospatial Analysis

4.4.1 Cropland land use / activity

To assess agricultural activity, the study applies the 3-Period TimeScan (3PTS) method developed by Boudinaud (2019) – see Appendix C for adapted script. This method summarizes vegetation dynamics by merging peak NDVI values from early, mid, and late growing seasons into a three-band composite. Sentinel-2 Level-1C imagery was used as input and processed in Google Earth Engine (GEE). NDVI values were calculated from the red (B4) and near-infrared (B8) bands (via the normalized difference between two bands) at 10-meter resolution and the maximum NDVI for each sub-period was used to generate the 3PTS products.

All processing steps, including NDVI calculation, cloud masking and 3PTS creation, were automated in Google Earth Engine (GEE), allowing efficient handling of the large Sentinel-2 datasets while capturing seasonal patterns in vegetation growth. The resulting tiff files of the GEE script were stored on Google drive and downloaded and added as raster layers in both ArcGIS Pro (3.2.0) and QGIS (version 3.34.10).

4.4.2 Built-up areas

Using the ESRI Living Atlas, the Impact Observatory LCLU time series dataset -as described in Section 4.2.2- will be used and processed in ArcGIS Pro.

The area for each region and period will be vectorized using the raster to polygon tool in ArcGIS Pro, and the built-up area in square kilometres for each period will be calculated.

4.4.3 Night-time Lights

Night-time light intensity is calculated using monthly NASA Black Marble radiance values, based on the VNP46A3 monthly product. This provides atmospherically and lunar-corrected radiance measurements.

Two indicators are derived:

- Total Night-time Light (TNL): Sum of radiance within each city buffer.
- Change Rate (CR): Year-to-year change in night-time lighting.

These metrics help identify disruptions in economic activity, population movements or settlement stability. This method is adapted from Zhang and Li (2025) who used this method for their research in the greater Sahel region.

The total night-time light (TNL) of a region is calculated as the sum of radiance values of all pixels within the study area:

$$\text{TNL} = \sum_{i=1}^{n} r_i \qquad (1)$$

where r_i is the radiance of pixel i and n is the total number of pixels. This measure provides an aggregate view of night-time lighting intensity across Mopti.

Year-to-year changes in night-time lights are calculated using the change rate (CR) formula:

$$CR = \frac{\text{TNL}_{i+1} - \text{TNL}_i}{\text{TNL}_i} \times 100\% \qquad (2)$$

This allows assessment of the growth or decline in night-time lighting, which can be linked to socio-economic shifts and conflict impacts over time (2017–2023).

4.4.4 Spatial Integration

To create and establish a framework for the statistical analysis, using ArcGIS Pro (3.2.0) and QGIS (3.34.10), the different datasets will be integrated into a unified geodatabase. The conflict events from the ACLED database will be spatially joined with the indicators as described in the previous paragraphs.

Given the logistical importance of the transit routes within and between the different regions for all events, a proximity analysis will be performed using a 3-kilometer buffer around all primary, secondary and tertiary road (not including trails). This 3-kilometre buffer also encompasses for any geo precision errors.

4.5 Statistical Analysis

Following the collection of the different datasets, statistical analyses will be performed. This will consist of a multi-method approach. This will be done to evaluate to what extent each of the derived remote sensing indicators are good predictors for the violence-related dynamics.

As explained in Section 3.3, the conflict in the study area is a complex adaptive conflict where violence causes more violence. As visualized in the layered conflict model (Figure 4), violent events are causing reinforcing feedback loops, that fuel the conflict. When faced with violence, communities have different coping mechanisms. Some might make arrangements with JNIM and agree on paying an extortion fee, while others might organise themselves into self-defence groups. The latter will result in more violence and increasing number of fatalities and even villages/settlements being burned down to the ground, further resulting in growing numbers of IDPs.

These changes will likely shift JNIM tactics, e.g. possibly resulting in more roadblocks and attacks on or near the major transporting routes. These blockades will also have an effect on fuel availability. In areas where the electrical grid is dependent on the availability and transportation of fuel, this will have a visible impact in the night-time light emissions. All of these dynamics trigger coping mechanisms that have to be considered when setting up the statistical analysis.

Due to the dynamic nature of the conflict, remote sensed indicators are influenced by many latent variables. Using linear regression with an Ordinary Least Squares (OLS) method would require the exogeneity assumption, which is the requirement that the error term is uncorrelated with the independent variables. In this context (given the dynamics of the conflict), however, many of the influential factors remain unquantifiable or unobservable. This will likely lead to omitted variable bias, and the error term would capture the effects of these missing variables.

Different methods were investigated and considered, looking into statistical methods for time-series datasets used in the fields of social and political science. In their article, Clarke and Granato (2005) discussed several models, their complexity and ability to address the dynamic nature of data.

One of the model structures considered for this study was an Autoregressive Integrated Moving Average (ARIMA). It was, however, deemed inappropriate for this study, as the objective is to identify causal spatial relationships across regions and is not suitable for forecasting a single temporal trend.

The three sorts of models that were selected for this study are Granger causality (Clarke and Granato, 2005), logistic regression (Estacio et al., 2023) and fixed effects (Farkas, 2005). See Table 4 for the methods used for each of the indicators. Each method will be further described after the table.

Table 4: Expected result and type of statistical testing per indicator

Indicator	Expectations and testing
Cropland activity	As an expected outcome of consolidation of control by JNIM, diminished land use for cropland activity will be visible in certain areas preceded by an increase in violent events and fatalities. Reduced cropland land use also predicts an increased number of IDPs. Statistical model: Logistic regression
Built-up area size	The growth of built-up areas of cities will show a (delayed) predictive relationship with IDP numbers. Statistical model: Granger causality
Night-time Light emission	The night-time light emissions will show a reduced stability, but overall increase due to expected migration pattern and the influx of IDPs due to violent events causing people to seek refuse in the relative safety of the cities. Statistical model: Fixed effects

4.5.1 Logistic Regression

Unlike linear regression, that predicts a continuous value, logistic regression predicts the probability (*P*) that the dependent variable (*y*) belongs to a specific category. These categories are binary. For example, we can find that such a model predicts in a certain instance, a probability of land abandonment being 0 or 1. A standard linear model is inappropriate for binary outcomes, as it can predict values below 0 and above 1. Using the logit link function (Estacio et al., 2023), logistic regression solves this issue and transforms the probability into the log-odds form, (see Logistic Regression formula below in Equation 3).

$$\ln \frac{P}{1 - P} = \beta_0 + \beta_1(\text{Violence}) \qquad (3)$$

Table 5: Components of Equation (3)

Component	Definition
P	Probability
ln	Natural logarithm
P / (1 – P)	The ratio of the probability of success to the probability of failure
β_0	The intercept, the predicted log-odds of the dependent variable when the independent variable is zero
β_1	The coefficient, the estimated magnitude and direction of the relationship between the predictor and the outcome

This ensures that the output of the model always stays between 0 and 1 (creating a Sigmoid curve). By calculating the Z-score, it can be determined how many standard deviations the coefficient is from the mean. Based on the resulting value, the likelihood of random change can be interpreted. If the absolute value of *Z* is larger than 1.96, a p-value smaller than 0.05 can be assumed.

$$Z = \frac{\text{Coefficient}}{\text{Standard Error}} \qquad (4)$$

Table 6: Components of Equation (4)

Component	Definition
Z	The significance test score (Z = β / SE) used to determine if the effect is statistically reliable
Coefficient	Expresses the estimated strength and direction of the effect of violence on land abandonment
Standard Error	Expresses the measure of statistical precision and uncertainty in the coefficient estimate

Lastly the McFadden's Pseudo R-squared will be calculated using the following equation, presented as Equation 5.

$$R^2{}_{McFadden} = \frac{\ln(\mathrm{L}_{full})}{\ln(\mathrm{L}_{null})} \tag{5}$$

Table 7: Components of Equation (5)

Component	Definition
R^2_{McFadden}	Pseudo R^2 in terms of likelihood of an event / variance
$\ln(\mathrm{L}_{full})$	Natural logarithm of the likelihood function including predictor (violence)
$\ln(\mathrm{L}_{null})$	Natural log-likelihood of the model without predictors

Both the Solver add-on in Microsoft Excel and SPSS will be used for this model.

4.5.2 Granger Causality

Granger causality is not actually measuring the causality between two variables in a direct sense. Instead, it tests if past values of one variable provide statistically significant information for predicting the current value of a second variable, looking beyond the past values of that variable.

This is a good method to assess if (specific) violent events have some causal link with cropland activity. To test this Granger causality uses restricted and unrestricted tests (Clarke and Granato, 2005) and uses a F-statistic to determine the significance of the causal links.

The formulas for both the unrestricted, restricted and F-statistics based on Clarke and Granato (2005) are presented below.

Unrestricted formula (Equation 6)

$$Y_{i,t} = \alpha + \beta Y_{i,t-1} + \gamma X_{i,t-1} + \epsilon_{i,t} \tag{6}$$

Restricted formula (Equation 7)

$$Y_{i,t} = \alpha + \beta Y_{i,t-1} + \epsilon_{i,t} \tag{7}$$

Table 8: Components of Equations (6) and (7)

Component	**Definition**
$Y_{i,t}$	Current value of indicator.
α	Constant term
$\beta Y_{i,t-1}$	The historical values of the indicator (built-up area)
$\gamma X_{i,t-1}$	The historical values of the other variable that is being tested in terms of predictive power (IDP numbers).
$\epsilon_{i,t}$	The random error term

F-statistic formula (Equation 8)

$$F = \frac{(\mathrm{RSS}_{restricted} - RSS_{unrestricted})/q}{\mathrm{RSS}_{unrestricted}/(\mathrm{n - k})} \tag{8}$$

Table 9: Components of Equation (8)

Component	**Definition**
$RSS_{restricted}$	The error – Residual Sum of Squares (RSS) – from the model that ignores the conflict variable.
$RSS_{unrestricted}$	The error (RSS) from the model that includes the conflict variable.
q	The number of restrictions (count of lags removed from the restricted model). In this case this refers to the number of lagged years.
n	The total number of observations.
k	The total number of parameters being estimated in the unrestricted model

As indicated in Table 4, this method will be used to examine causal links between IDP numbers and built-up area size. The directionality of those links will also be tested. Microsoft Excel using the Data Analysis ToolPak will be used as tool to run the equation. In Excel a panel data set will be created with columns for region, year, built-up area size, number IDPs, one year lagged built-up area size and one year lagged number of IDPs.

4.5.3 Fixed Effects Model

As explained by Farkas (2005), fixed effects models are a form of regression analysis. It is a method used in a panel data analysis to control for variables that do not change over time, like for example, the different regions that can be observed over a longer period and the differences between those regions.

Looking at night-time light, due to the annual variations and temporal shocks like fuel shortages, a regular fixed effects model would potentially introduce bias, as this does not account for these shocks.

To adapt for these potential problems, Zhang and Li (2025) suggest using a two-way fixed effects model for this specific kind of data, which includes both regional-fixed effects and temporal-fixed effects. The correlation between the night-time light values and number of conflict events was tested. The regression equation used is as follows:

$$\ln\left(\mathrm{TNL}_{jt}\right) = \beta_0 + \beta_1 \mathrm{In}\left(\mathrm{conflict}_{jt}\right) + \eta_j + \theta_t + \varepsilon_{jt} \qquad (9)$$

Table 10: Components of Equation (9)

Component	Definition
$\ln(\mathrm{TNL}_{jt})$	Dependent variable (night-time light radiance) for region j at time t.
$\ln(\mathrm{conflict}_{jt})$	Independent variable (ACLED conflict events)
β_0	Constant term
β_1	The coefficient (degree of correlation)
η_j	The region-fixed effects
θ_t	The year-fixed effects
ϵ_{jt}	Random error term

Both Microsoft Excel using the Data Analysis ToolPak and SPSS will be used as tool to run the equation. A panel data set will be created with columns for region, year, conflict numbers and night-time light radiance values.

4.6 Summary

This chapter has described the research design, data sources, geospatial methods and statistical techniques used to analyse violence-related spatial change in the study area. By integrating remote sensing datasets with conflict records and applying a structured analytical workflow, the study provides a methodological foundation for assessing how patterns of violence manifest in the landscape.

This has been done by implementing a workflow for the study follows a sequential structure, consisting out of:

1. Data acquisition
2. Pre-processing and harmonization
3. Derivation of cropland, night-time lights and built-up area indicators
4. Spatial integration with conflict events
5. Statistical testing of hypotheses

This sequence ensures that the conceptual framework, geospatial analysis and statistical models are fully integrated. In the next chapter the empirical results generated through this approach will be presented, interpreted and discussed.

5. Results

In this chapter, the results of both the geospatial and statistical analyses described in the previous chapter will be presented.

5.1 Cropland activity

For each region 3PTS composites were created using GEE. The composites have three bands that per (10 by 10 meter) cell hold the highest NDVI value for each of the three time periods. Red for period 1 (day 166 to day 228), green for period 2 (day 228 to 259) and blue for time period 3 (day 259 to 284).

The main staple crops in the Mopti region are Millet and Sorghum, which during the growing season peak at a NDVI value of about 0.60. According to the Food and Agriculture Organization (FAO, n.d.) Millet and Sorghum require a yearly precipitation range of respectively 300 to 600mm and 300 to 750 mm. (Sissoko et al., 2022) showed that in the Mopti region the yearly precipitation range has met these conditions since the early 1980's. Looking at the individual regions in the study area for the year 2016-2023, the CHIRPS rainfall data as presented in Table 11 shows that these regional values also fall within the range that meets these main crop requirements.

Table 11: Yearly precipitation in mm in selected zones in study area.

	2016	2017	2018	2019	2020	2021	2022	2023
Bankass	603	561	705	584	687	602	722	626
Bandiagara	605	573	637	526	701	545	694	569
Douentza	465	463	470	448	514	388	587	427
Koro	494	491	531	467	543	444	598	490

As will be discussed in Section 6, several attempts were made using unsupervised classification and a rule-based approach to differentiate cropland from natural vegetation. As these attempts have not resulted in a usable approach, the choice was made to conduct a visual comparison (year-to-year change) of the yearly 3PTS composites.

The 3PTS composite with an RGB band linked to each of the 3 time periods for the maximum NDVI values, where the colours indicate:

- Black: No activity;
- White/grey: Stable values in all periods;
- Red: Peak in period 1 and low values in other periods;
- Green: Peak in period 2 and low values in other periods;
- Blue: Peak in period 3 and low values in other periods;
- Yellow: Activity in period 1 and 2, but no activity in period 3;
- Cyan; Little activity in period 1, but activity in period 2 and 3.

Using a linear contrast stretch the 3PTS script also amplifies the differences between areas that have similar NDVI values throughout the 3 periods and areas that have dominant (significantly higher) NDVI values in one or two periods. This results in croplands having more vibrant and saturated colours compared to natural vegetation that is visualised in unsaturated/pale colours. Making it possible to visually single out and distinguish croplands (that mostly also have distinct boundaries) from natural vegetation.

Based on these patterns during the agricultural crop cycle, in table 12 the different land use classes are described with their corresponding colour range. Based on this information can be used for a visual interpretation of the 3PTS composites, the differences are clearly visible in both figure 7 and 8, with figure 8 clearly showing the difference in colour saturation.

Table 12: 3PTS composite colour interpretation/classification

Colours	Classification (description)
Vivid Dark Blue	Active late-season cropland These fields under cultivation, with crops like Millet and Sorghum. These colours are defined by late season maximum biomass indicating crops have reached maximum canopy right before harvest.
Vivid Purple / Pink-Red	Active early-/mid-season cropland This represents crops that matured or peak early in the seasonal cycle.
Bright Cyan / Turqoise	Intense village adjacent cropland Represents highly managed and fast growing crops, mainly in direct vicinity of villages.
Muted Pink, Grey-Green and Beige	Natural vegetation and fallow lands Visible as “blurry” background landscape that represents natural Sahelian grasslands and wild shrubs and lands that are in transition, that mainly also lack sharp agricultural boundaries.
Deep black clusters	Built-up areas This represents non-vegetated surfaces with constantly low NDVI values like houses, tin roofs and roads.

In the 3PTS composites presented as Figures 7 and 8, the villages of Bobosso and Doukoro are shown in 2017 and 2023. In 2017, cropland activity is visible in the composites in both villages, while in 2023, no cropland activity is visible. Table 13 provides the minimum and maximum NDVI values for the 3 periods of the growing season in the Bankass region.

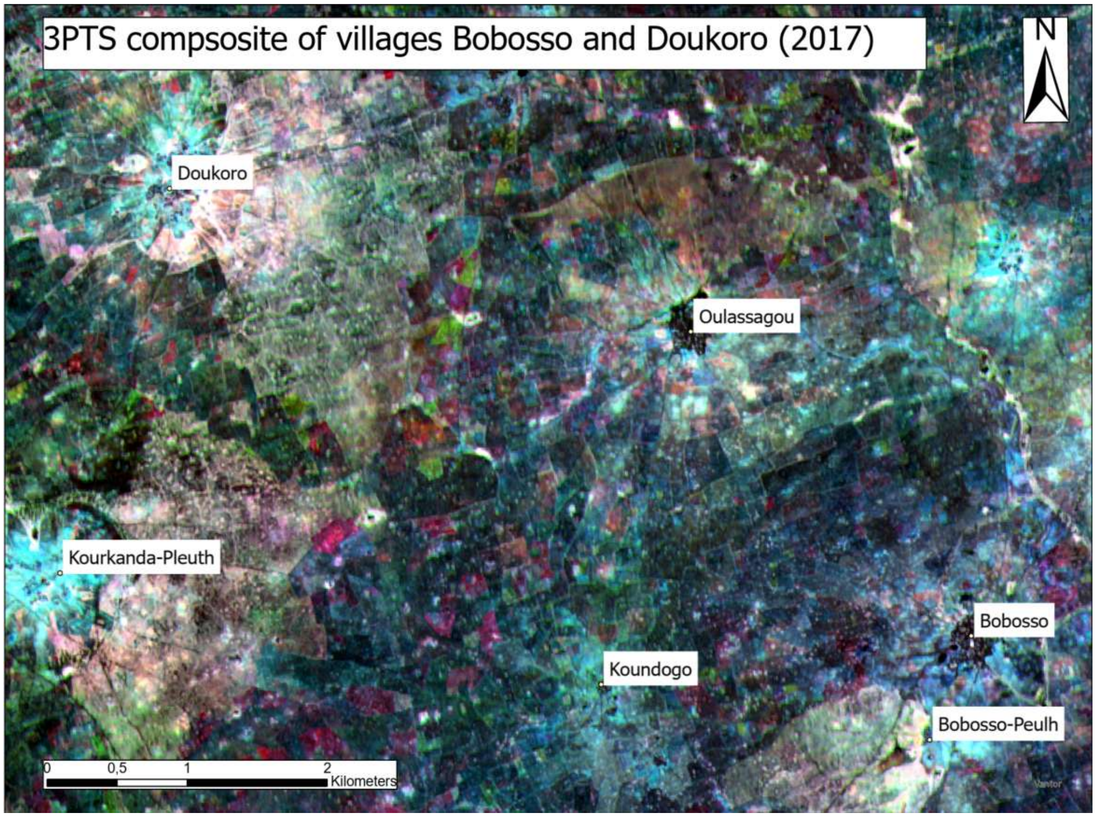

Figure 7: Villages Bobosso and Doukoro in 2017 (Bankass region) circled in red.

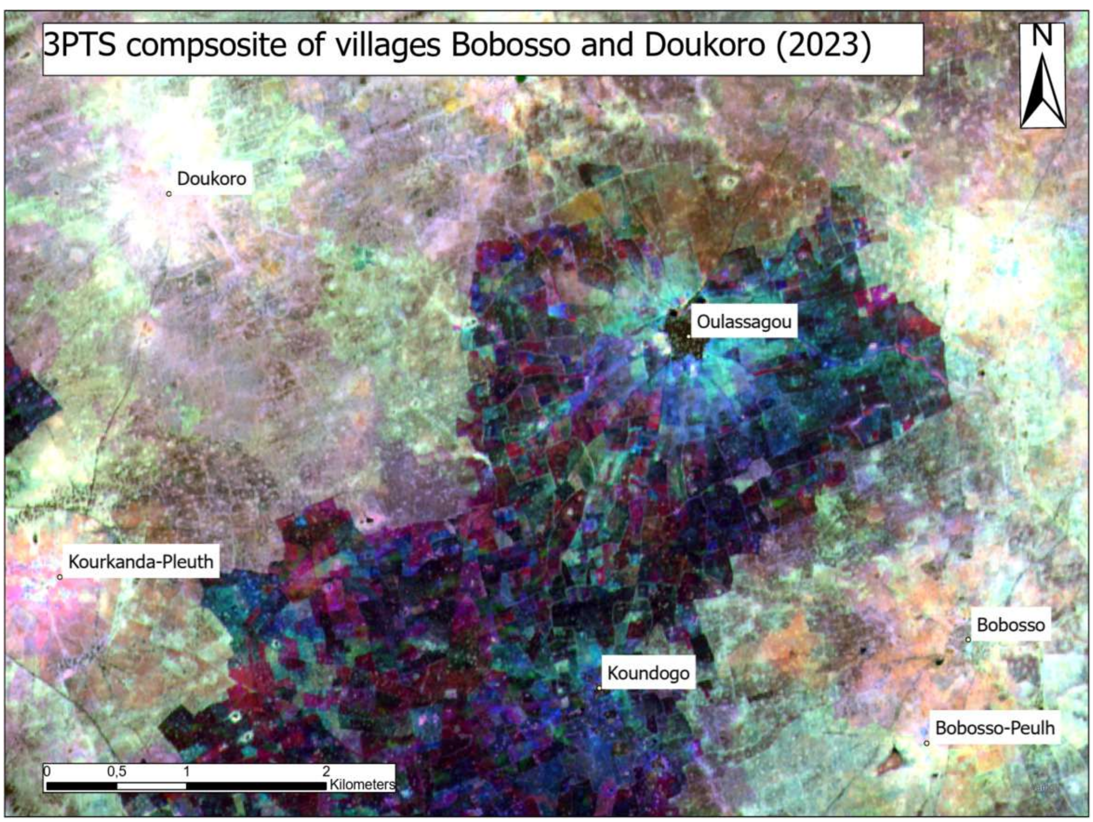

Figure 8: Villages Bobosso and Doukoro in 2023. Villages/settlements seem abandoned.

Table 13: Minimum and maximum NDVI values during the three periods growing season (Bankass region).

Band	**2017**		**2023**	
NDVI	**Min**	**Max**	**Min**	**Max**
Red (period 1 – day 166 to 228)	0.1379310	0.7473226	0.0745903	0.5841584
Green (period 2 – day 228 to 259)	0.1310712	0.7720739	0.1168590	0.6220821
Blue (period 3 – day 259 to 284)	0.1526791	0.7269880	0.1283179	0.5794494

The results correspond with the ACLED events that have been reported in the area. After the violent events in 2019, the 3PTS composites show a recovery in 2021, and the effect of the new violent events in 2022 is clearly visible in cropland activity in the 2023 composite.

These are the major reported events reported for these villages in the ACLED database:

- On 2 January 2019, presumed Dogon militiamen attacked the Fulani village of Bobosso and burned huts.
- On 22 July 2022, suspected JNIM militants attacked the Dogon village of Bobosso (Bankass, Mopti). Nine people were killed including eight men and one woman, others went missing, and houses were burned.
- On 15 January 2023, soldiers attacked the village of Doukoro (Bankass, Mopti). Two persons, including an elderly man and a child from the Fulani community were killed, houses burned, and livestock seized.

See Appendix B for the high-resolution images (2019 versus 2024) of the centre of the village Bobosso. They show the total destruction of all houses in the village in 2024. Looking at the images, many other villages in the area suffered the same fate, but events were not always recorded as events in the ACLED database. More about this can be found in Section 5.5.

The year-to-year change of cropland activity based on visual comparison for each area is presented in table 14 below.

Table 14: Changes in cropland activity in different regions

	2017	**2018**	**2019**	**2020**	**2021**	**2022**	**2023**
Bandiagara	o	o	-	-	+	o	+
Bankass	o	o	--	--	+	-	--
Douentza	o	o	--	o	-	o	+
Koro	o	-	--	+	o	+	o

Legend for these values:

--	major decrease (≥25%)
-	minor decrease (<25%)
o	stable / no significant change
+	minor increase (<25%)
++	major increase (≥25%)

The 3PTS method is previously validated by Boudinaud & Orenstein (2021), which also includes field data for the study area of this study. In this study, the presented results are checked against high-resolution imagery and reported ACLED events.

The visual inspection of the 3PTS composites did not only show a decrease or increase in farmland activity, but also changes in the patterns. In several areas, the fields furthest from a village/settlement seemed to be abandoned, while around a village all possible cropland seemed to be cultivated. Showing fields to be closer together compared to earlier years with a maximum distance from the village of approximately 2 kilometres.

Before performing the logistic regression, the data in Table 14 was translated into two binary classes: one class for (minor and major) decreases, and one class for all other values. Based on the binary data the result for year+1 is a model with the following parameters and resulting values:

- Intercept: -3.25504
- Coefficient: 0.065786
- Sum Log-likelihood: -12.9936
- Odds ratio: 1.067998
- Standard error: 0.033
- Z-score: 1.98

This results in a p-value of approximately 0.047 and a pseudo R^2 value based on the Equation 5 (McFadden) of 0.149. SPSS also provides Nagelkerke value of 0.241.

With a Z-score exceeding 1.96 and a p-value of 0.047, the result is statistically significant at a 95% confidence level, ruling out random change and rejecting the null hypothesis. The pseudo R^2 value of 0.149 provides a substantial fit. The negative intercept value resulting from the logistic regression model indicates that the chance of land abandonment is low if there were no violent events against civilians. The model shows that the odds of land abandonment occurring increase by 6.8% for each additional violent event.

5.2 Built-up areas

The 9-class LCLU from Impact Observatory based on Sentinel-2 Level-2A imagery with a 10-meter resolution appeared not to be able to reliably detect smaller rural cities and settlements. In those areas, the materials used for building the houses consist of materials that have a spectral signature that is very similar to bare ground or rangeland. The LCLU classified all of these areas as rangeland.

Due to these limitations, only the built-up area of the main city in each region was derived from the classification method. In Figures 9A – 9D, the perimeter of the built-up area of the city Bandiagara for the years 2017 to 2023 is shown in red.

Comparing 2017 to 2023, the built-up area for Bandiagara is 3 km^2 versus 5.5 km^2, respectively. This is a growth of more than 80%. The other cities in the study area also show a significant growth in built-up area, as shown in Table 15. Presented values are in square kilometres (km^2).

Looking at high-resolution imagery (see example of Bandiagara in Appendix A), significant new built-up areas are clearly visible in all cities; see Table 15. This is in accordance with the results of the applied LCLU classification. A remark must be made that when comparing the result with high-resolution imagery, there is a huge difference in built-up density for the cells classified as built-up area. Some cells only show limited/questionable built-up characteristics, whereas others show dense built-up characteristics. This will be further discussed in the next chapter.

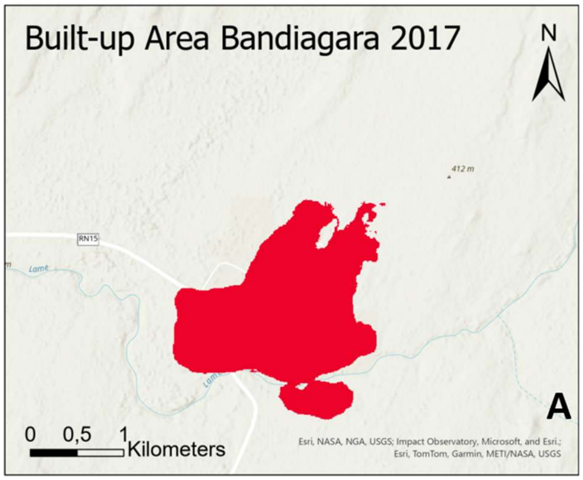

Figure 9A: Bandiagara Built-up area 2017

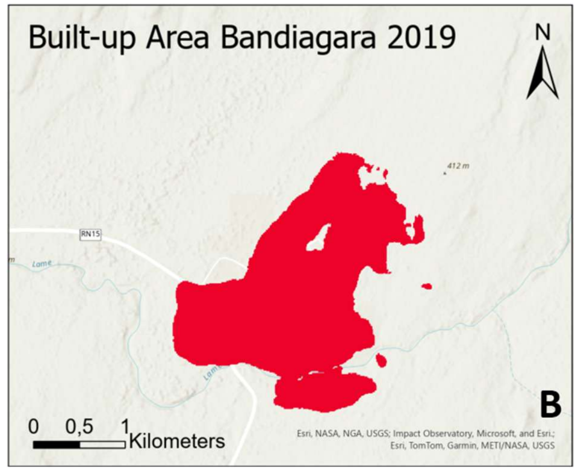

Figure 9B: Bandiagara Built-up area 2019

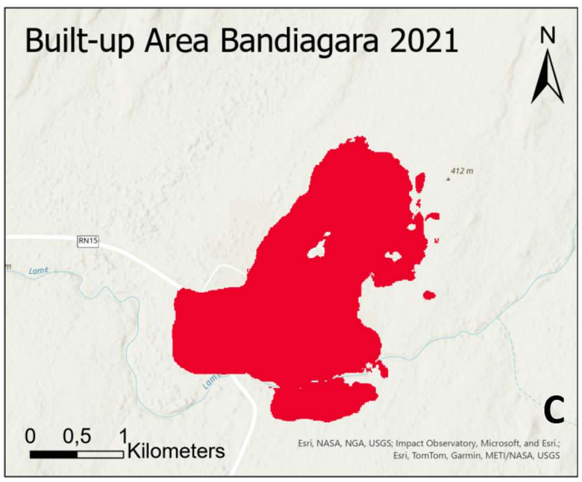

Figure 9C: Bandiagara Built-up area 2021

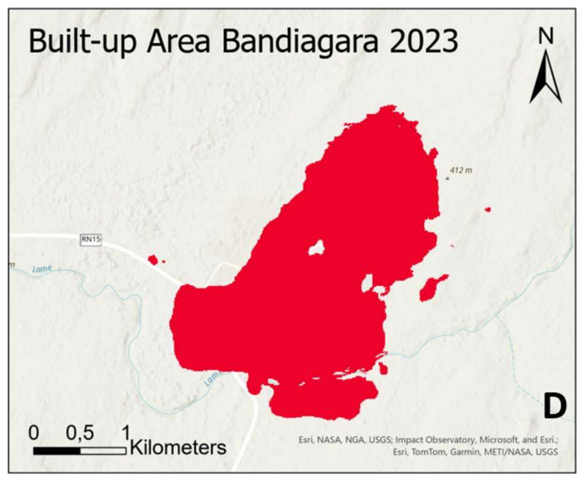

Figure 9D: Bandiagara Built-up area 2023

Table 15: Built-up area 2017-2023 in square kilometres

City	2017	2019	2021	2023
Bankass	2.2	2.9	3.3	4.3
Bandiagara	3.0	3.8	4.4	5.5
Douentza	3.9	4.3	5.0	5.5
Koro	5.3	7.4	8.2	9.6

The LCLU algorithm used has a reported (Karra et al., 2021) performance at 80% precision (user's accuracy) and 95% recall (producer's accuracy) for built-up areas, and there is a 20% error of commission and 5% error of omission. This translates into potentially 20% of cells incorrectly being classified as built-up areas and 5% that should be classified as built-up areas that are not.

In terms of an F1 score (Equation 10):

$$F1 - score = \frac{2 \text{ x Precision x Recall}}{\text{Precision + Recall}} \tag{10}$$

The resulting F1-score is (2 × 0.80 × 0.95) / (0.80 + 0.95) = 0.8686

This F1 score is considered to be a good result, but in general it overestimates the built-up area. Visually comparing the results in this study against high-resolution imagery, the classification performed within the expected parameters.

The number of IDPs were derived from data provided by HDX per region. The values based on the HDX reports for the four regions are presented in the graph shows as Figure 10.

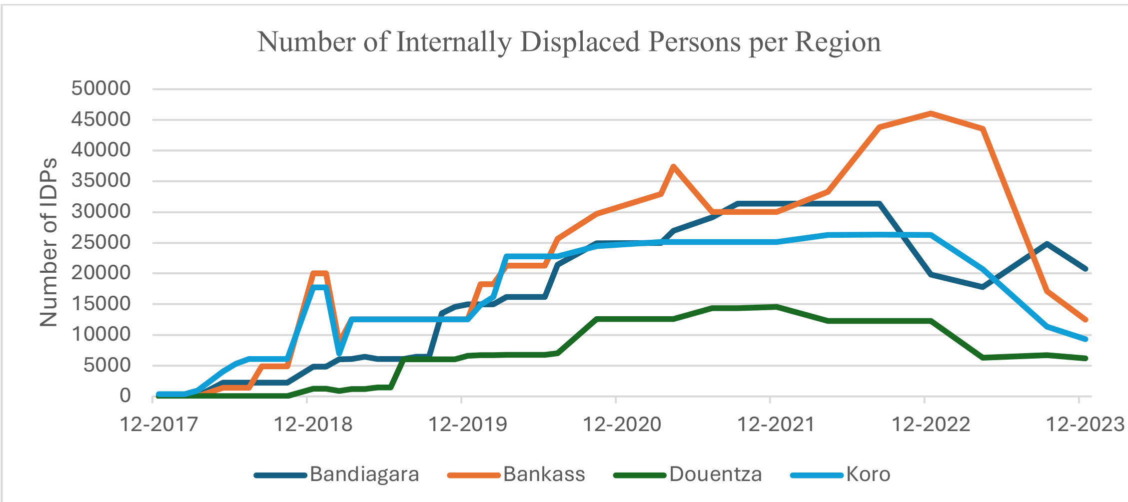

Figure 10: Graph with number of internally displaced persons per region 2017-2023 based on HDX data.

The drop in the second half of 2023 in Bankass and Koro is partly due to a correction in the numbers, as explained in the IOM report "sur les Mouvements de Populations" (2023). This report mentions the implementation of a new biometric registration system, which uncovered thousands of duplicate registrations that were corrected in the September 2023 numbers.

Granger causality between number of IDPs and built-up area size was tested using the statistical model as described in Section 4.5.2.

First Equation 7 (Restricted formula) was run, resulting in the following values:

- R^2 value: 0.988175
- Residual Sum of Squares (RSS): 1.033985
- Number of Lags (q): 1-year lag
- Number of Observations (n): 24
- Degrees of Freedom: 22
- Number of Parameters (k): 2

Next Equation 6 (Unrestricted formula) was run, resulting in the following values:

- R^2 value: 0.988182
- Residual Sum of Squares (RSS): 1.033372

- Number of Lags (q): 1-year lag
- Number of Observations (n): 24
- Degrees of Freedom: 21
- Number of Parameters (k): 2

Based on these results using Equation 8 the F-statistic value was determined. Resulting in an F-statistic value of 0.013

Using the Excel function F.DIST.RT using a F-distribution based on the F-statistic value and taking into consideration the number of Lags degrees of Freedom the P-value was calculated as being 0.91.

The model was also tested in the other direction, between Built-up area size and IDP numbers, which provided the following resulting values:

First Equation 7 (Restricted formula) was run, resulting in the following values:

- R^2 value: 0.18773
- Residual Sum of Squares (RSS): 1954426272
- Number of Lags (q): 1-year lag
- Number of Observations (n): 24
- Degrees of Freedom: 22
- Number of Parameters (k): 2

Next Equation 6 (Unrestricted formula) was run, resulting in the following values:

- R^2 value: 0.207249
- Residual Sum of Squares (RSS): 1907463183
- Number of Lags (q): 1-year lag
- Number of Observations (n): 24
- Degrees of Freedom: 21
- Number of Parameters (k): 2

This resulted in a F-statistic value of 0.541655 and a derived P-value of 0.47.

With a P-values in both directions well above 0.05, the result is statistically not significant, making it impossible to reject the null hypothesis based on this result.

5.3 Night-time light emissions

The areas outside the main cities in the study area show no or only faint emissions of night-time lights. The values are too low for the sensor to detect them or to be able to distinguish the values from noise. That's why in this study the choice was made to zoom in to the night-time lights for the main regional cities in the study area.

Based on the yearly Total Night-time Light (TNL), the year-to-year night-time light emissions change rate (CR) was determined for each city based on the footprint as described in Section 4.2.2. The result is shown in Figure 11. The presented values for each year are based on what was found for the previous year.

The values show an unstable development of the yearly night-time light emissions. For each city, the average night-time light emissions value was calculated based on the footprint. This approach is taken in order to present the development of the monthly values for each city in a reasonable comparable fashion. The results (deviations from the average for each specific city) are shown in the graph in Figure 12;

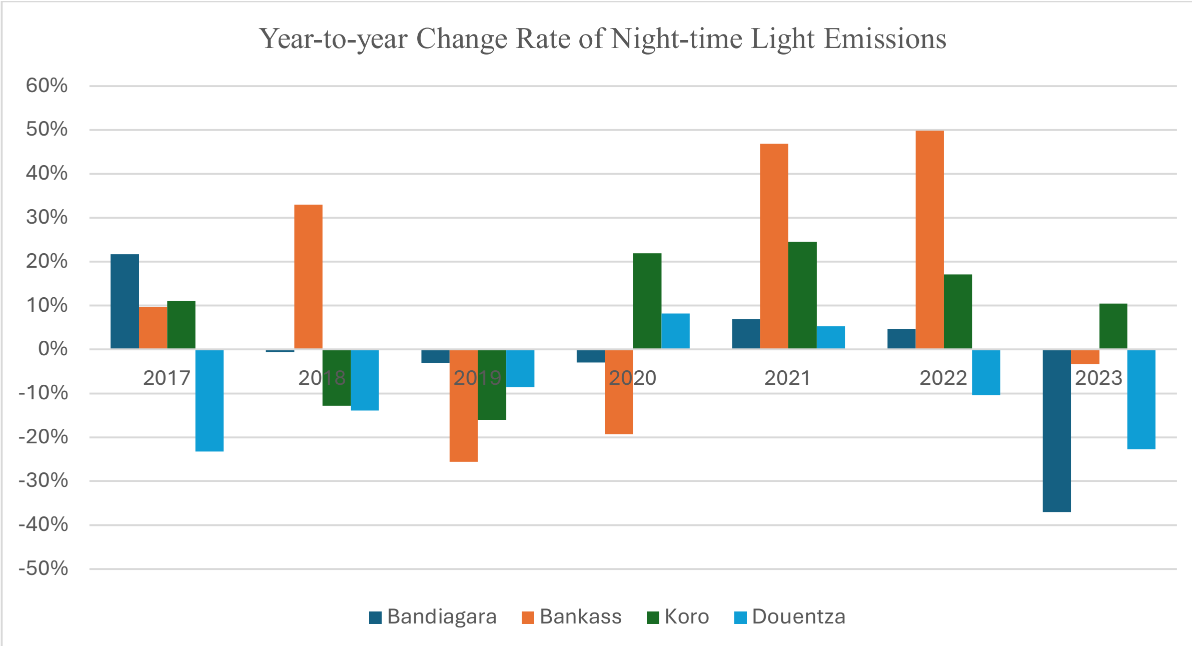

Figure 11: Year-to-year change rate of night-time light emissions.

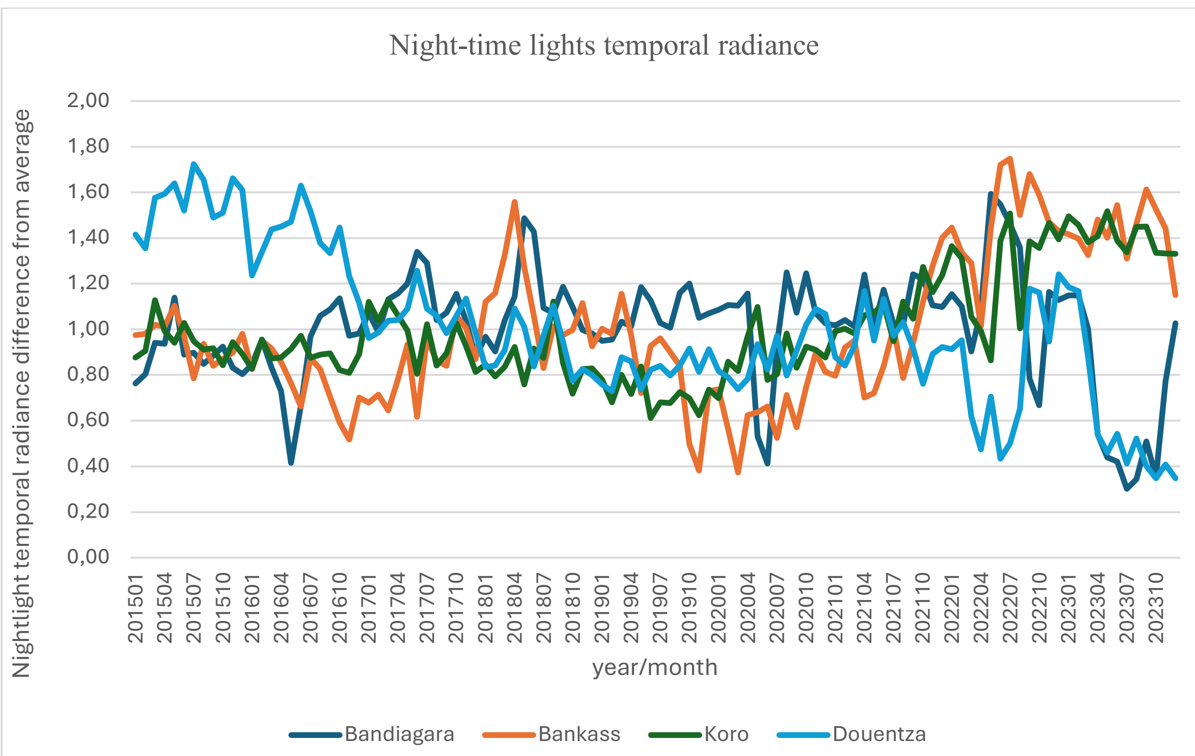

Figure 12: Graph with night-time light values from 2016-2023.

The graph in Figure 12 shows notable fluctuations, with several lows in 2016, 2022 and 2023, especially for Bandiagara.

For each of these events in Bandiagara, a search was conducted for any relevant news reports on these fluctuations. L'Observatoire (2016) reported structural financial problems at Énergie du Mali (EDM) resulting into power cut offs. Other news reports (Traoré, 2022 and Africanews, 2023) continuing problems in 2022 and 2023 at EDM with maintenance and meeting the growing demands, resulting in power cuts. As these reported events match the lows in the graph, it can be reasonably reasoned that these events are related. Looking into the differences between Bandiagara and the other cities, is clear that Bankass, Koro and Douentza rely less on the EDM infrastructure, as they have their own local (hybrid) networks.

Another explanation for fluctuation could be a lack in data quality. The Black Marble User Guide (NASA, 2021) states that pixels that have significant cloud contamination could receive the quality flag "poor quality". As most cloud cover is expected during the rainy season starting in May and ending in October, values in the quality band for these months were checked. Out of the total 95 cells that were monitored each month, at most 2 cells were flagged as "poor quality". This does not indicate any significant problems due to data quality.

Using a two-way fixed effect model adapted from Zhang and Li (2025), which includes both regional-fixed effects and temporal-fixed effects, the correlation between the night-time lights values and number of conflict events was tested (see Equation 9 as presented in Chapter 4).

As explained in Section 4.4.3 TNL_{jt} and $conflict_{jt}$ were logarithmically treated. Using the yearly TNL values from 2015 to 2023 for all four regions results in a sample size of 36 (N=36).

The two-way fixed effect model resulted in the following values:

- Coefficient: 0.142757
- R^2 value: 0.937496
- P-value: 0.040

This indicates that a 1% increase in conflict events results in a 0.14% increase in night-time light emissions in the cities. With a P-value below 0.05, the result is statistically significant at a 95% confidence level, this would in theory rule out random change and reject the null hypothesis. However, with a R^2 value well above 0.90 the result seems "to good to be true" and will be further discussed in the next chapter Discussion.

In addition to running this statistical model for all conflict events, the model was also used looking at specific conflict events. The two most mentionable are the selection of all conflict events that are classified as violence against civilians and are away for the roads as explained in Section 4.4.3 and with a selection on all conflict events that resulted in fatalities.

The values for a selection on all conflict events classified as violence against civilians and 3 km away from the roads are:

- Coefficient: 0.059954
- R^2 value: 0.926754
- P-value: 0.043
- N=36

The values for a selection on all conflict events that resulted in fatalities are:

- Coefficient: 0.08871
- R^2 value: 0.935711
- P-value: 0.059
- N=36

Zooming in on these specific conflict events didn't provide an improvement on the overall model fit as the R^2 values remained consistently high (above 0.9). Also, the coefficients for violence against civilians away from roads and fatalities were notably lower than found in the general model.

5.4 Conflict Event Data

As described in the previous chapter, all of the 2273 events that took place in the study area during the 2017-2023 time period were visualized in ArcGIS Pro as point data. The events in the ACLED database were compared to the results of this study. Specifically, focusing on the agricultural activities, not all events appear to be recorded in the ACLED database.

In Section 5.1.1, events are described that took place in the villages of Bobosso and Doukoro. The ACLED events recorded for that area match the changes that are detectable using the 3PTS method. The 3PTS composites uncovered many places that suffered the same fate as the villages of Bobosso and Doukoro, but do not show up in the ACLED database.

An example is an unnamed settlement 3 kilometres north of the town of Diallassagou. If we look at the images available in Google Earth Pro (Figures 13 and 14), we can see that between May 2017 and June 2019, all the huts around the settlement and most of the houses in the settlement were destroyed. The 3PTS composite shows no agricultural activity in this area in 2019.

To rule out geo-precision errors, which could occur within the ACLED database, a wider search was conducted to find these events, but no record was found.

During this search and contact with ACLED, records showed similar events in villages nearby that are recorded in the ACLED database based on news reports. France24 reported in June 2022 that suspected jihadists killed more than 130 civilians in and around the town of Diallassagou. ACLED confirmed these events are registered under the following event IDs: MLI6869, MLI6870 and MLI6871.

Figure 13: High resolution image of the area 3km north of Diallassagou May 2017 (Source Google Earth Pro)

Figure 14: High resolution image of the area 3km north situation after June 2019 (Source Google Earth Pro)

6. Discussion

In this chapter, the results of this study will be discussed by comparing the results to other studies and through a critical analysis of the results and data quality.

6.1 Limitations

Several limitations in regard to the methodology should be acknowledged and will be discussed in this chapter:

- The quality of the Sentinel-2 imagery might be reduced due to cloud cover or atmospheric effects.
- The Black Marble radiance values may be affected by sensor noise of lunar effects, regardless of correction.
- Determining changes in agricultural land-use and built-up areas based on a visual interpretation of the 3PTS composites involves a degree of subjective interpretation.
- The 3PTS method relies on the NDVI for creating the composites, these may be influenced by variability in rainfall and/or atmospheric conditions rather than changes due to human behaviour alone.
- ACLED event data might contain reporting bias, missing events and uncertainty of the event location.
- The 10-meter resolution of Sentinel-2 and the spectral similarities between traditional building materials and surrounding soil in the study area, may lead to under detection of those built-up areas using LCLU algorithms.

6.2 Evaluation of Remote Sensing Indicators as Proxies

As presented in Chapter 2, the aim of this study is to assess whether remotely sensed socio-economic indicators can be reliably used as identifiers of violence-related spatial change in Central Mali. The three indicators being investigated are cropland activity, built-up area and night-time lights.

6.2.1 Cropland activity indicator

Using the 3PTS method and visually compare the year-to-year cropland changes was not the first choice for this study. Preferably, an existing LCLU method would have been used to determine the changes in cropland activity. As explained in Section 4.2.2, this was not a viable option due to the poor performance of these methods in the study area.

Using a visual interpretation of the 3PTS composites in this study is a primary methodological limitation. Although a visual analysis allows for the interpretation of expert contextual knowledge and avoids pixel-misclassification errors common to automated machine learning algorithms in the Sahelian environment, it introduces inherent challenges regarding subjectivity and scalability.

First, visual interpretation is subject to operator bias, as the delineation of abandoned versus active cropland boundaries relies heavily on the analyst's qualitative perception of colour thresholds, saturation and spatial patterns. This can introduce inconsistencies when replicating the study over larger geographic scales or across different landscape boundaries.

Second, environmental noise, such as localized variations in for example soil moisture can alter the background values of the 3PTS composites. Without automated machine learning techniques, distinguishing between naturally induced crop failures and conflict driven land abandonment might require a high reliance on secondary qualitative sources (e.g. conflict event databases or local testimonies). Future research could address these limitations by training deep learning models, specifically on the 3PTS colour trajectories to standardize the inference process.

It was assessed if it was possible to not only visually distinguish the natural vegetation from agricultural activity, but also to achieve this through using either a supervised or unsupervised classification method. The attempt of applying an unsupervised approach within the Koro region are shown in Figures 15A and 15B. Figure 15B shows active cropland cells in black and all other cells in white.

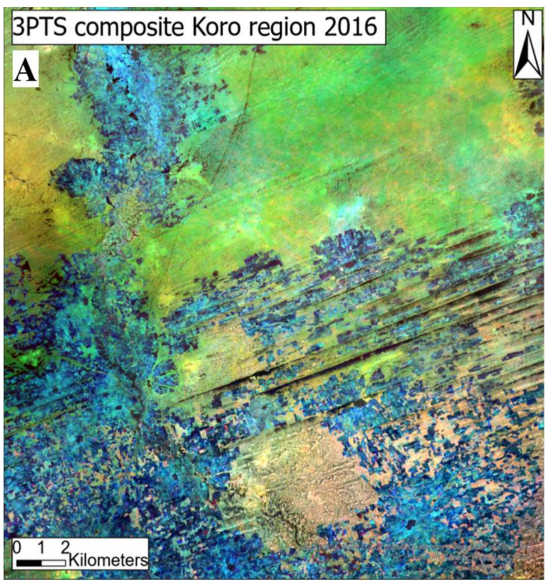

Figure 15A: 3PTS composite for 2016.

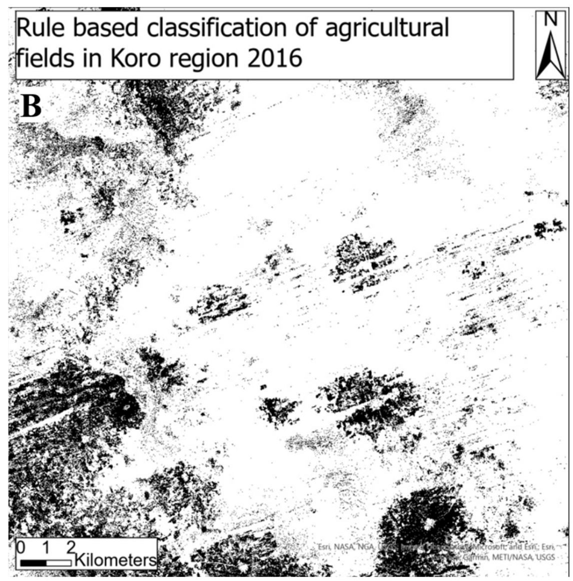

Figure15B: Resulting crop fields

This method provided promising results for a given year as shown in Figure 15B, but due to the year-to-year variation in the spectral signatures (not static) appeared to not be scalable to other years in the study.

Additionally, a rule-based approach as described by Wang et al. (2015) was attempted based on the following values and logical rules:

- The amplitude between the maximum and minimum NDVI values during the three time periods.
- The peak of the NDVI values in the second period compared to the first.
- A minimum increase of the maximum NDVI values in the third period compared to the second.

This did not provide a solution for this study, even though a similar approach provided good results for Wang et al. (2015). The key difference is that Wang et al. (2015) used a supervised classification method, as is used in most LCLU studies. Another example of such a study is the study conducted by Eklund et al. (2017) for the classification of cropland areas in Iraq and Syria.

Like this study, Eklund et al. (2017) used the seasonality and specific growth patterns to distinguish between natural vegetation and cropland. They chose a supervised classification method using Landsat imagery and MODIS NDVI and used referenced RGB images to visually identify land use classes at a resolution of 30 meters. Due to an average field size of 125000 square meters, the MODIS pixel size (250 x 250 meters) was deemed to be sufficient for selecting training samples in their study area.

Looking at the study area in this study, the average field size is much smaller, about 25000 square meters, as described by Karnan and Sebesvari (2024). This is why, as explained in Section 4.2.2, the Sentinel-2 imagery at 10 m resolution was preferred over Landsat imagery at 30-meter resolution due to the average plot size. This makes it more challenging to find enough training samples that cover at least one MODIS pixel.

Applying the methodology as described by Eklund et al. (2017) would have been a good approach for this study. This, however, would have entailed investing considerable time and resources that were neither available, nor were the focus of this study.

Based on the findings as presented in this paragraph, the original developer of the 3PTS script (Boudinaud, L., 2019) was contacted. Since the publication the 3PTS method they further developed the 3PTS script and attempted running a supervised classifiction based on the 3PTS composites. These attempts have not provided results so far and further research is needed. Another topic discussed was the validation proces of the 3PTS method. Due to the security situation in Mopti, the researchers were not able able to collect as much field data as is needed to conform to statistical norms. As an extra measure, the results were also validated by focus groups from key actors in agriculture in both Mopti and Bamako. While these focus group provided necessary qualitative grounding, the sample size remains limited by regional insecurity. Future studies should focus on expanding this dataset to provide the extra data points needed for a more complete and statistically solid validation.

Applying a logistic regression model for statistical testing as described in Section 5.1 provided a promising result, indication significant odds of related land abandonment due to violence against civilians. Due to the limited sample size and use of visual interpretation method these results should be seen as an indicative result and a good starting point for further research.

The 3PTS method provides humanitarian organizations an easy to apply and use tool to generate yearly composites. These can be used as a “triage” tool to visualize the areas most affected and help in prioritizing the humanitarian aid efforts.

6.2.2 Built-up area indicator

Section 4.2.2 explains that the 9-class LCLU classification method used in this study does not differentiate between low- and high-density built-up areas. Other models, like the paid 11-class LCLU classification method developed by Impact Observatory do make this distinction, but they are offered at a commercial rate of $2 per square kilometre. Although this model can show both low- and high-density built-up areas, the total area identified as built-up area would not change, still slightly overestimating the overall built-up area size.

A study conducted by the Centre for Information Resilience (CIR) used a different methodology, which also leads to a difference in growth of the built-up area. In their study (CIR, 2024), built-up area growth in 3 of the 4 cities that are assessed in this study were also assessed. Their methodology consists of a visual comparison of the presence of built-up area in each individual cell for the years 2020, 2023 and 2024 using high resolution imagery at a resolution of 3 meters.

Their conclusion for the different cities was:

- Bandiagara: 2020-2022 + 0.13 sq. km yearly average growth and + 0.05 sq. km growth in 2023.
- Bankass: 2020-2022 + 0.08 sq. km yearly average growth and + 0.05 sq. km growth in 2023.
- Koro: 2020-2022 +0.25 sq. km yearly average growth and + 0.02 sq. km growth in 2023.

These growth numbers are significantly lower when compared to the growth numbers based on the 9-class LCLU classification based on 10 meter resolution Sentinel 2 data used in this study. Figure 16 from the CIR report shows Bandiagara with, shown in yellow, growth between 2020 and 2022, and, shown in blue, the growth in 2023.

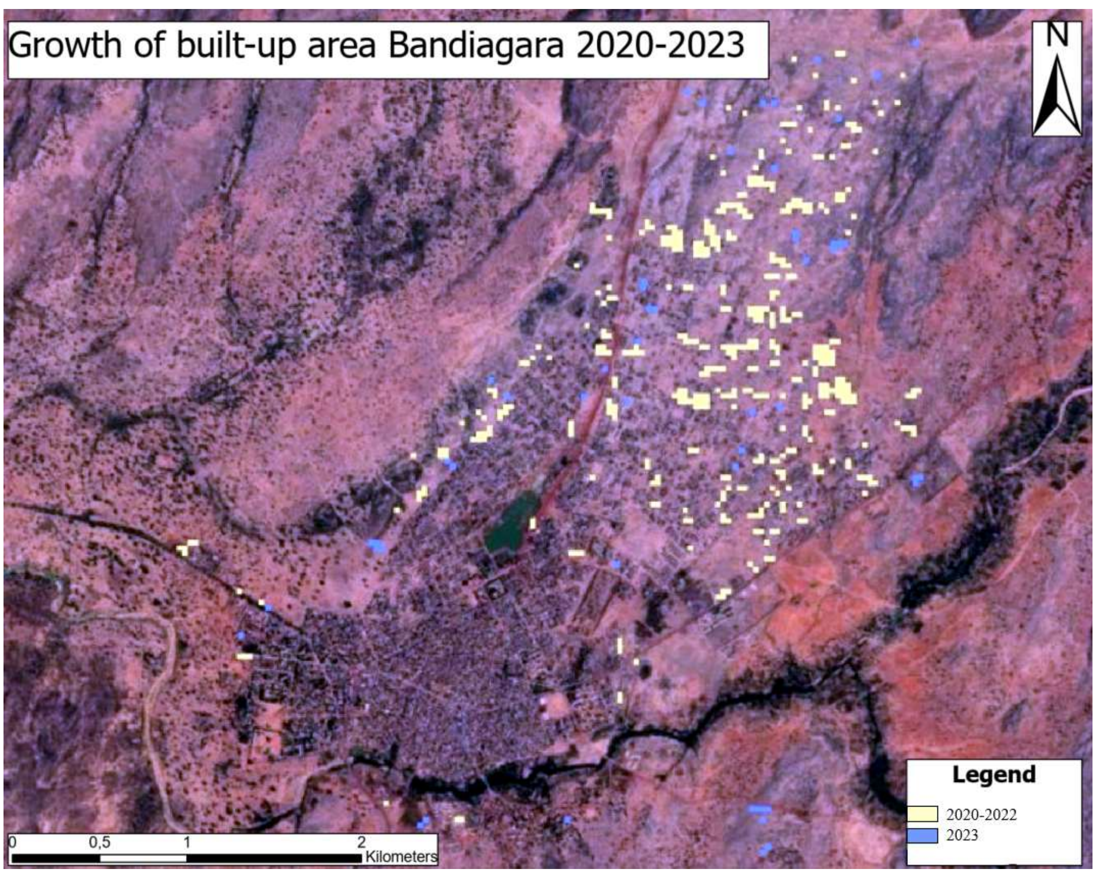

Figure 16: urban growth in Bandiagara 2020-2023 according to CIR report: Satellite imagery analysis of Malian population displacement dynamics.

The difference is that in the CIR study, for each individual picture, the change in built-up area was visually determined at a 3 meter cell resolution, and the method used in this study uses a deep learning AI algorithm that also uses the spatial context of the surrounding cells to determine the classification of a specific cell as described in Chapter 4.

Looking at the development and growth rate of the built-up area of a city, the major factors are population growth and the trends in urbanisation. According to the Institute for Security Studies (2025), the population growth rate in Mali is 3.3%. Starting with 9.2 million people in Mali in 1990, the population number in 2023 has already gone up to 23.8 million. The forecast is that this will grow further, reaching 40 million people in the early 2040s. At the same time, more and more people are leaving rural areas to (try to) establish a better life in the cities. These patterns are a significant driver of urbanisation. Looking at these factors, the growth of the built-up areas in the cities according to the CIR numbers aligns with these broader demographic trends.

One of the other questions is where do the IDPs stay, and what is their contribution to the growth of built-up area. It was assumed their presence would result in growth of built-up area as explained in Chapter 2. But according to the International Organization for Migration (IOM, 2023) a lot of internally displaced persons seek refuge with family or friends, like the woman whose testimony was quoted in the introduction of Chapter 3. Those who are not lucky enough to find refuge with friends or family will first end up finding shelter in community buildings such as the Bandiagara museum. IOM (2023) reports approximately 500 internally displaced persons from 60 households that were residing at the Bandiagara Museum in 2022. They were moved to the first shelters (in the north of Bandiagara – see Figure 17). More shelters were added later. These temporary shelters are visible in the high-resolution imagery, which indicates the presence of IDPs and/or refugees.

Figure 17: Area to the north of Bandiagara where IDPs are temporarily housed (Google Earth Pro 2025), with in frame picture taken by the International Organization for Migration (2023) of the temporary housing.

This shows that many IDPs that have suffered a loss in livelihood while leaving their home, and lack the immediate means to regain self-sufficiency. The fluctuations in the IDP numbers also show that a significant number of IDPs try to return to their place of origin or eventually move on. One can reason that those who stay need to recover their livelihood first. Following this logic, this will result in a time lag between actual IDP numbers rising and being able to detect a growth in built-up area.

This would also explain why the results presented in Section 5.2 showed that IDP numbers do not provide predictive information for future built-up area development and built-up area growth is not a good indicator for violent related spatial change in the study area. An R^2 value well above 0.9 would indicate that the model used would have “solved” the complexity of the relationship between IDP numbers and growth of built-up area in the cities. Also looking at the high P values showing no statistically significant result, the more logical explanation is that the sample size is too small, and it will take IDPs more time to reestablish their livelihood.

6.2.3 Night-time lights indicator

The NASA Black Marble VNP46A3 monthly composite product is used in this study. It is important to distinguish this product from Top-of-Atmosphere products like the VNP46A1 product (Román et al., 2022). TOA data products contain significant noise for lunar cycles and atmospheric aerosols. Ch, that is refined through sophisticated Bidirectional Reflectance Distribution Function (BRDF) adjustments and atmospheric correction.

Despite these corrections the observed seasonal fluctuations suggest that environmental factors could still remain influential. Seasonal variations in vegetation canopy and ephemeral hydrological changes can modulate the surface's optical properties, which would result in altered detected radiance regardless of actual changes in human-generated light. Surface reflectance may also vary due to the albedo effect: During the winter, the ground will be dry and have a higher reflectance, in comparison to the wet season, when the soil contains more moisture and is darker.

These conditions and the expected variation in radiance levels, are also visible in values as presented in Section 5.1.3. They show a peak in radiance during the boreal winter that coincides with the dry season in Mali and in summer the higher NDVI values coincide with lower radiance values.

The values for the Mopti region as discussed with the Level-1 and Atmosphere Archive & Distribution System (LAADS) from NASA. They confirm that dust and other aerosols can indeed influence NTL observations by scattering or blocking the emitted light, which may lead to lower observed radiance values under certain atmospheric conditions, but there are no anomalies to be considered, specific for the Mopti region, that would have an abnormal impact on the final NTL signal. This is confirmed by Román et al. (2022). They conclude that the methods for making atmospheric corrections that account for aerosols including dust are effective. These methods consist of applied radiative transfer modelling with an additional boxplot method and removal of outliers.

Based on the assumption that these methods are effective, the impact of dust and other aerosols is negligible. It is therefore vital to consider changes in socio-economic human behaviour and seasonality as the main factors of influence.

Where Zhang and Li (2025) proved a negative and significant correlation between TNL and the number of conflicts in a region, this study showed a positive correlation between TNL and conflicts events. The difference is that this study did not focus on the total night-time lights in the entire region but focussed on the night-time light emissions for defined cells within the city polygons. This aligns with the assumption that IDPs seek refuge in the cities, which relatively offer more safety.

As mentioned in Section 5.3 the fixed effects regression analysis yielded a remarkably high coefficient of determination (R^2). This indicates a strong fit, but such a high value in the context of the complexity explained in this study, is remarkable and not very realistic in social science specifically also looking at the small sample size. The limited number of observations was spread across the dummy variables, resulting in a risk of overfitting. Based on the results in this study, this risk can be classified as a high risk and therefore question the predictability of the model as used in this study. Further research could focus on a larger sample size consisting of data from more cities over a longer period.

6.3 The Data Quality Challenge

According to Human Inference (n.d.), the six dimensions of data quality are:

- Consistency; the data must be consistent in all aspects.
- Accuracy; the data must be current and correct.
- Completeness; all of the relevant data has to be included.
- Validity; the data must be compliant to established policies and rules.
- Uniqueness; the data must be unique rejecting redundancies.
- Timeliness; the data must be available, current and accessible.

Although the data in the ACLED database is consistent and the validity is checked through the described methodology/safeguards, there is no difference represented with respect to the severity of the events. The same importance is giving to both a small and large impact event. Also, this study showed that not all events are registered in the database, indicating there are gaps in the completeness, as only events are registered that are reported and can be validated.

A check against the Uppsala Conflict Data Program (UCDP) data shows that the number of reported fatalities in the ACLED database in the study area from 2017-2023 is 5741, compared to the 3227 fatalities (best estimate) reported in the UCDP database. Sundberg and Melander (2013) describe in their article that the UCDP database provides a better accuracy for those events that lead to fatalities. In both databases, no references can be found destruction of certain villages around the town of Diallassagou. So of the events were reported by France 24 (2022). According to France 24, these reported events led to the killing of more than 130 civilians. It is unknown why other events are missing, in villages that seems to have suffered the same fate.

Using the 3PTS composites, this study also uncovered missing events in the ACLED database as reported in Section 5.1. These findings align with those of Boudinaud and Orenstein (2021) and Zhang and Li (2025), who also report missing events in the ACLED database.

Looking at the aim of this study and considering these facts about the events in the ACLED dataset, it is challenging to establish significant correlations between the different indicators.

6.4 Socio-Economic Impacts and Human Needs

As described in Section 3.3, the study area has been conducted at a location in a phase of contestation since 2017, with the events resulting in "a complex adaptive conflict system," in which a small change can generate an unpredictable outcome.

Looking at the 3PTS composites and ACLED event data, it is visible that the impact of the conflict to villages like Bobosso and Doukoro is enormous. At the same time, the village of Oulassagou (located right between Bobosso and Doukoro) seems unaffected. Data alone cannot explain these differences; human behaviour and the enabling factors, as described in the layer conflict model, (Figure 4) are key factors.

As described by Maslow's hierarchy of needs (1943), a human has basic physiological and safety needs. If these are not met, people go into "survival mode", resulting in a predictable cycle of violence. Both insurgents and the population adapt to changing conditions, with varying outcomes. While faced with a threat by insurgents, the coping mechanisms can differ: Whereas in village A, people might flee from the emergent violence, those from village B might instead try to organize self-defence, while those from village C might try to negotiate.

With remote sensing, it is possible to identify villages like Oulassagou that seem unaffected in a region that is affected heavily by the violence. Remote sensing cannot answer why this is the case but can identify those areas where field research / interviews could potentially provide the answer to these questions.

6.5 The role of GEOINT in Conflict Monitoring

Zheng and Li (2025) concluded their paper on the assessment of the central Sahel crisis by night-time lights imagery with some advice for future researchers. They mentioned that more research is needed to analyse the night-time light patterns in the urban areas and include research on the effects of conflict on agricultural activity.

Eklund (2017) advises that further research on the topic of conflict and land systems, should focus on developing a framework for understanding which factors (like socio-economic and environmental) play a role in detectable changes in land use.

This study focussed on those aspects, providing an additional insight in conflict research in the central Mali/Sahel region. This study showed a good direction further research could focus on in attempting to bridge the gaps using integrating multi-temporal LCLU data with socio-environmental variables. This approach could be used as a framework for transforming raw geospatial observations into a spatial triage tool for conflict monitoring, to assess where humanitarian interventions are most needed.

7. Conclusions

This study explored the use of open-source geospatial intelligence (GEOINT) and remote sensing indicators. Specifically cropland activity, built-up area and night-time light emissions to reveal and monitor violence-related spatial dynamics in Mopti region of Mali between 2017 and 2023. By evaluating these physical indicators alongside conflict records, the research provides a valuable and practical insights into how landscape transformations can reflect an underlying human security crises, even when field access is entirely restricted by active conflict.

7.1 Indicator Performance and Findings

Rather than operating as definitive predictive evidence, the geospatial indicators in this study offer a foundational and explorative insight into to a highly complex and adaptive conflict system. The three indicators yielded distinct levels of utility.

<u>Cropland Activity</u>

The 3-Period TimeScan (3PTS) method emerged as a practical and insightful tool for visually identify changes in landuse. By tracking the vegetation during the agricultural crop cycle, the 3PTS composites successfully isolated patterns of agricultural land abandonment. In localized areas like the Bankass region (e.g. the villages of Bobosso and Doukoro), visible cropland abandonment directly corresponded to severe and recorded insurgent attacks on village. While the logistic regression indicated that a rise in civilian violence increases the odds of land abandonment, these numbers must be treated as indicative. The constraint of a small regional sample size means this approach is best utilized as a visual monitoring baseline rather than a definitive predictive instrument.

<u>Built-up Areas</u>

Horizontal urban expansion was clearly captured across all primary regional hubs using the Impact Observatory's deep-learning Land Classification Land Use (LCLU) dataset. For example the footprint of Bandiagara expanded by over 80% during the study period. Granger causality failed to establish a statistically significant predictive relationship between these expansions and internally displaced person (IDP) numbers. Qualitative context uncovered why. Demographic records show that many IDPs initially integrate into existing structures (moving in with friends of family) or shared community spaces, which do not translate immediately into an expanding built-up area footprint. Thus, most probable cause for urban built-up area growth in this context is reflected by long-term, macroeconomic urbanization trends rather than active, short-term displacement caused by conflict.

<u>Night-time Lights (NTL)</u>

The two-way fixed effects (TWFE) model demonstrated a relationship between conflict frequencies and localized urban light fluctuations. However, the model returned an exceptionally high coefficient of determination. In socioeconomic conflict research, a near-perfect fit of this magnitude indicates overfitting, due to the model's fixed-effect dummies that are capturing systemic regional variances and technical parameters rather than an active, clean correlation with real-time conflict intensity. NTL remains a valuable operational proxy for broader infrastructure stability and monitoring municipal power grids. For example signalling disruption due to fuel shortages or maintenance issues matching with localized light drops in Bandiagara. In this study the statistical output of this indicator should be interpreted cautiously as a technical artifact of the model setup.

7.2 Addressing Methodology Gap

One of the most useful outcomes for researchers attempting similar studies is the documentation of a significant completeness gap in traditional conflict event databases. By cross-examining the 3PTS composites against the ACLED registry, this study uncovered hidden conflict signatures. In an unnamed settlement three kilometres north of Diallassagou, satellite baselines revealed total structural destruction and complete cropland abandonment by in 2019, with no corresponding event existing within the validated ACLED point database for that timeframe.

This reinforces the argument that remote sensing does not merely supplement event reporting, but it uncovers unverified or unrecorded territorial consolidation by insurgent actors. For humanitarian and security organizations, this workflow provides a functional "spatial triage" capability. It allows operators to cheaply scan vast, non-permissive environments, identify anomalous livelihood collapses and prioritize field-based aid interventions or deeper open-source investigation.

7.3 Final Reflections and Future Research

The objective of this study was to assess whether remote sensing and open-source geospatial data could reveal and reliably identify remote sensing indicators to track violence-related spatial change in Central Mali between 2017-2023.

This study has provided some insights into the complexity and dynamics of the conflict, which transformed a region that had previously found a delicate balance between farming and herding communities into a region in constant conflict. By integrating remote sensing with conflict event data and human security theories, this study has showed that geospatial intelligence (GEOINT) can provide a “spatial triage” capability that event databases like ACLED cannot provide by themselves.

This study showed that spatiotemporal indicators can be derived using accessible remote sensing tools and imagery. Regarding cropland activity, the 3PTS method provides multi-temporal RGB composites visualizing the agricultural growing cycle. Through this method and corresponding events in the ACLED database, affected areas are spotted where, apparently, the local agriculturally based livelihood has collapsed due to conflict induced abandonment. These spatial signatures represent more than just land abandonment, they are also indicators for deteriorating conditions for the inhabitants of these areas. Who become more dependent on humanitarian aid and often struggle to provide in their basic needs.

Night-time light emissions serve as a dual indicator, not only show the effects of the conflict itself, but also the broader signs of economic instability and disruption. The two-way fixed effects model provided a technical result due to the models setup and limited datapoints.

While the growth of the city's built-up area is evident, the statistical correlation between built-up area growth and conflict remains more complex. This complexity is likely also caused by significant time lags between the displacement itself, the diverse adaptive responses and the re-establishment of a person's livelihood that allows him/her to build a house. To elevate the model into a robust statistical predictor, future research must expand both the spatial sample size (e.g., incorporating wider cross-border regions across Burkina Faso and Niger) and the temporal scale to better account for multi-year lag effects between violence, migration and physical constructions visible as built-up.

Understanding the impact of the conflict requires looking beyond "dots on a map". It involves gaining a deep understanding of the specific dynamics in an area that play a role. As the conflict evolves and is fuelled, the cascading effects result in a complex adaptive system, where everyday life is disrupted and endangered, resulting in the loss of livelihoods for many people.

From a GEOINT perspective, the spatial temporal indicators presented in this study offer a "bottom-up" view of conflict, by focusing on the disruption of livelihoods rather than just kinetic events. For humanitarian organizations, these indicators can act as a cost-effective triage tool, allowing them to identify the most vulnerable areas and enabling them to prioritize their aid efforts.

To further enhance the findings of this study, future research is recommended into developing a tailored LCLU algorithm specifically for the unique spectral characteristics of the Mopti region. This could help to automate detecting spatial changes in agricultural land use. This could also contribute further to investigating the temporal lag between violence and detectable spatial change. Additionally, the developed workflow could be applied to other regions in the Sahel (with appropriate parameterization), which could validate broader regional usability of this set of approaches as a monitoring tool for humanitarian and security organizations.

Understanding why certain villages seemingly exhibit higher resilience, despite similar exposure to insurgency actors, remains a vital question for future field-based and geospatial integration studies.

References

Armed Conflict Location & Event Data Project (ACLED). (2023, March 1). *How does ACLED code and review data to ensure quality?* https://acleddata.com/methodology/how-does-acled-code-and-review-data-ensure-quality

Africanews. (2023, May 12). *Mali power cuts squeeze businesses, households*. Africanews. https://www.africanews.com/2023/05/12/mali-power-cuts-squeeze-businesses-households

Avtar, R., Komolafe, A. A., Kouser, A., Singh, D., Yunus, A. P., Dou, J., Kumar, P., Gupta, R. D., Johnson, B. A., Thu Minh, H. V., Aggarwal, A. K., & Kurniawan, T. A. (2020). *Assessing sustainable development prospects through remote sensing: A review.* Remote Sensing Applications: Society and Environment, 20, 100402. https://doi.org/10.1016/j.rsase.2020.100402

Baba, B. (2023, December). *Conflicts between farmers and herders in Mali: A review of the dynamics and issues in the Mopti Region* (*Fragility, Conflict and Migration Case Study)*. International Livestock Research Institute (ILRI). https://www.ilri.org

Bonkoungou, B., Bossa, A. Y., van der Kwast, J., Mul, M., & Sintondji, L. O. (2024). Inner Niger Delta inundation extent (2010–2022) based on Landsat imagery and the Google Earth Engine. *Remote Sensing, 16*(11), 1853. https://doi.org/10.3390/rs16111853

Boudinaud, L., 2019. Google Earth Engine script for 3PTS composites for cropland change interpretation. https://code.earthengine.google.com/c1c5529b8f9b997a8ec2afe12d3dc95d

Boudinaud, L., & Orenstein, S. A. (2021). *Assessing cropland abandonment from violent conflict in central Mali with Sentinel-2 and Google Earth Engine*. *The International Archives of the Photogrammetry, Remote Sensing and Spatial Information Sciences, XLVI-4/W2-2021*, 9–15. https://doi.org/10.5194/isprs-archives-XLVI-4-W2-2021-9-2021

Burton, J. W. (2024). Needs theory (1997). In D. J. Dunn, H. G. Brauch, & P. Burton (Eds.), *John W. Burton: A pioneer in conflict analysis and resolution* (Vol. 33, pp. 245–256). Springer. https://doi.org/10.1007/978-3-031-51258-2_23

Chauzal, G., & van Damme, T. (2015). *The roots of Mali's conflict: Moving beyond the 2012 crisis*. Netherlands Institute of International Relations (Clingendael), Conflict Research Unit. https://www.clingendael.org/sites/default/files/pdfs/The_roots_of_Malis_conflict.pdf

Centre for Information Resilience. (2024, March 15). *Satellite imagery analysis of Malian population displacement dynamics*. https://www.info-res.org/app/uploads/2025/01/Satellite-imagery-analysis-of-Malian-population-displacement-dynamics.pdf

Clarke, H. D., & Granato, J. (2005). Time series analysis in political science. In K. Kempf-Leonard (Ed.), *Encyclopedia of social measurement* (Vol. 3, pp. 829–837). Elsevier. https://doi.org/10.1016/B0-12-369398-5/00321-2

Collier, P., & Hoeffler, A. (2004). Greed and grievance in civil war. *Oxford Economic papers*, *56*(4), 563–595. https://doi.org/10.1093/oep/gpf064

Deininger, K. W., Ali, D. A., Kussul, N., Lemoine, G., & Shelestov, A. (2024). *Micro-level impacts of the war on Ukraine's agriculture sector: Distinguishing local and national effects over time* (Policy Research Working Paper No. 10869). World Bank. https://doi.org/10.1596/1813-9450-10869

Eklund, L., Degerald, Michael, Brandt, Martin, Prishchepov, Alexander V., & Pilesjö, Petter. (2017). How conflict affects land use: Agricultural activity in areas seized by the Islamic State. *Environmental Research Letters*, *12*(5), Article 054004. https://doi.org/10.1088/1748-9326/aa673a

Eklund, L., Mohr, B., & Dinc, P. (2024). Cropland abandonment in the context of drought, economic restructuring, and migration in northeast Syria. *Environmental Research Letters*, *19*(1), Article 014077. https://doi.org/10.1088/1748-9326/ad1723

Estacio, I., Sianipar, C. P. M., Onitsuka, K., Basu, M., & Hoshino, S. (2023). A statistical model of land use/cover change integrating logistic and linear models: An application to agricultural abandonment. *International Journal of Applied Earth Observation and Geoinformation*, *120*, Article 103339. https://doi.org/10.1016/j.jag.2023.103339

Famine Early Warning Systems Network. (2015, August). *Mali livelihood zone descriptions*. https://fews.net/west-africa/mali/livelihood-description/august-2015/print

Farkas, G. (2005). Fixed-effects models. In K. Kempf-Leonard (Ed.), *Encyclopedia of social measurement* (pp. 45–50). Elsevier. https://doi.org/10.1016/B0-12-369398-5/00161-4

Food and Agriculture Organization. (n.d.). *Crop information: Sorghum, Millet, and Cowpea water management*. Land & Water Division. https://www.fao.org/land-water/databases-and-software/crop-information/en/

France 24. (2022, June 20). *Suspected jihadist kills more than 130 civilians in central Mali*. https://www.france24.com/en/africa/20220620-suspected-jihadist-kills-more-than-130-civilians-in-central-mali-official-says

Galtung, J. (1969). *Violence, peace and peace research.* Journal of Peace Research, 6(3), 167–191. https://doi.org/10.1177/002234336900600301

He, T., Zhang, M., Xiao W., Zhai, G., Wang, Y., Guo, A., & Wu, C. (2023). Quantitative analysis of abandonment and grain production loss under armed conflict in Ukraine. *Journal of Cleaner Production*, *412*, Article 137367. https://doi.org/10.1016/j.jclepro.2023.137367

Hishe, S., Gidey, E., Zenebe, A., Bewket, W., Lyimo, J., Knight, J., & Gebretekle, T. (2024). The impacts of armed conflict on vegetation cover degradation in Tigray, northern Ethiopia. *International Soil and Water Conservation Research*, *12*(4), 635–649. https://doi.org/10.1016/j.iswcr.2023.11.003

Homer-Dixon, T. F. (1999). *Environment, scarcity and violence*. Princeton University Press.

Human Inference. (n.d.). *6 Dimensions of Data Quality*. https://www.humaninference.com/en/inspiration/6-dimensions-data-quality

Insecurity Insight. (2024, August). *Conflict-Induced Food Insecurity in Mali: Examining the Links between Conflict and Hunger*. https://insecurityinsight.org/wp-content/uploads/2024/08/Conflict-Induced-Food-Insecurity-in-Mali-August-2024.pdf

Institute for Security Studies. (2025). *Mali: Geographic futures — Current path*. African Futures & Innovation. https://futures.issafrica.org/geographic/guide.pdf?geography=ML&topic=02-current-path

International Crisis Group. (2020, November 9). *Reversing Central Mali's descent into communal violence* (Africa Report No. 293). https://www.crisisgroup.org/africa/sahel/mali/293-reversing-central-malis-descent-communal-violence

International Organization for Migration. (2023, January 3). *IOM Mali supports IDPs in Ménaka and Bandiagara*. IOM Regional Office for West and Central Africa. https://rodakar.iom.int/news/iom-mali-supports-idps-menaka-and-bandiagara

International Organization for Migration (IOM), Oct 27 2023. *DTM Mali — Rapport sur les Mouvements de Populations (Septembre 2023).* IOM, Mali. https://dtm.iom.int/fr/reports/mali-rapport-sur-les-mouvements-de-populations-septembre-2023

Impact Observatory. (n.d.). *Maps for Good classes*. Retrieved January 2, 2026, from https://www.impactobservatory.com/monitor/maps-for-good-classes/

Kafando, W. A., & Sakurai, T. (2025). Effects and mechanisms of armed conflict on agricultural production: Spatial evidence from terrorist violence in Burkina Faso. *Journal of Agricultural Economics*, *76*(1), 24–44. https://doi.org/10.1111/1477-9552.12613

Karra, K., Kontgis, C., Statman-Weil, Z., Mazzariello, J.C., Mathis, M., and Brumby, S.P., "Global land use / land cover with Sentinel 2 and deep learning," *2021 IEEE International Geoscience and Remote Sensing Symposium IGARSS*, Brussels, Belgium, 2021, pp. 4704-4707. https://doi.org/10.1109/IGARSS47720.2021.9553499.

Karnan, M., & Sebesvari, Z. (2024). Livelihood restoration and recovery in the context of coastal land use/land cover change: A systematic literature review. *Coastal Futures*, *2*, 100025. https://doi.org/10.1016/j.cosf.2024.100025

Krampe, F., Kreutz, J., & Ide, T. (2025). Armed conflict causes long-lasting environmental harms. *Environment and Security*, *4*(1), 3–17. https://doi.org/10.1177/27538796251323739

Krätli, S. (2021). *Farmer–herder conflict in sub-Saharan Africa?* International Institute for Environment and Development (IIED). https://www.iied.org/sites/default/files/pdfs/2021-01/10208IIED.pdf

L'Observatoire. (2016, October 5). *L'eau et l'électricité : La souffrance des Maliens atténuée*. *Maliweb*. https://www.maliweb.net/economie/developpement/leau-lelectricite-souffrance-maliens-attenuee-1811802.htm

Li, X., Li, D., Xu, H., & Wu, C. (2017). Intercalibration between DMSP/OLS and VIIRS night-time light images to evaluate city light dynamics of Syria's major human settlement during Syrian Civil War. *International Journal of Remote Sensing*, *38*(21), 5834–5854. https://doi.org/10.1080/01431161.2017.1331476

Maslow, A. H. (1943). A theory of human motivation. *Psychological Review*, *50*(4), 370–396. https://doi.org/10.1037/h0054346

Mounkaila, Y., Moussa, B., & Garba, I. (2021). NDVI, a Proxy for the Associated Millet and Cowpea Growth Stages in the Sahelian Zone. *European Journal of Applied Sciences, 9*(5), 299–310. https://doi.org/10.14738/aivp.95.11002

National Aeronautics and Space Administration (2021). *Black Marble user guide (Collection 2.0)*. VIIRS Land Team. https://viirsland.gsfc.nasa.gov/PDF/BlackMarbleUserGuide_Collection2.0.pdf

Ng'ang'a, S. K., Diarra, L. Notenbaert, A. and Herrero, M. 2013. Coping strategies and vulnerability to climate change of households in Mali. CCAFS Working Paper no. 35. CGIAR Research Program on Climate Change, Agriculture and Food Security (CCAFS). Copenhagen, Denmark. Available online at: www.ccafs.cgiar.org

Nsaibia, H., Beevor, E., & Berger, F. (2023, October). *Non-state armed groups and illicit economies in West Africa: JNIM*. ACLED & GI-TOC. https://acleddata.com/system/files/2025-06/jnim-non-state-armed-groups-and-illicit-economiesin-wwest-africa-gi-toc-acled-october-2023.pdf

Organisation for Economic Co-operation and Development (OECD). (2021). *Pastoralist violence in North and West Africa* (Report). OECD Publishing. https://www.oecd.org/content/dam/oecd/en/publications/reports/2021/07/pastoralist-violence-in-north-and-west-africa_541e23b6.pdf

Prishchepov, A. V., Müller, D., Dubinin, M., Baumann, M., & Radeloff, V. C. (2013). Determinants of agricultural land abandonment in post-Soviet European Russia. *Land Use Policy*, *30*(1), 873–884. https://doi.org/10.1016/j.landusepol.2012.06.011

Provoost, M. (2019, August 31). *Symbiosis in the Sahara and Sahel.* Social Science Research Network. https://doi.org/10.2139/ssrn.4704133

Roberto, W. M., Closs, M. B., & Ronconi, G. B. A. (2013). *The situation in Mali*. UFRGSMUN | UFRGS Model United Nations Journal, 1, 71–97. Retrieved from https://d1wqtxts1xzle7.cloudfront.net/37423024/The-Situation-in-Mali-libre.pdf

Román, M. O., Wang, Z., Sun, Q., Kalb, V., Miller, S. D., & Molthan, A. (2022). NASA's Black Marble Multiangle Nighttime Lights Temporal Composites. *IEEE Geoscience and Remote Sensing Letters*, *19*, 1-5, Art no. 2501305. https://doi.org/10.1109/LGRS.2022.3176616

Sissoko, P., Synnevåg, G., & Aune, J. B. (2022). Effects of low-cost agricultural technology package on income, cereal surplus production, household expenditure, and food security in the drylands of Mali. *AIMS Agriculture and Food*, *7*(1), 22–36. https://doi.org/10.3934/agrfood.2022002

Statafric East Africa-U (2023). *Hiswaca U-ESMF: Pastoralism and livestock in Mali* [Report]. Statafric / African Union. https://statafric.au.int/sites/default/files/2023-04/hiswaca_u-esmf_p178497_05apr2023_cleared.pdf

Sundberg, R., & Melander, E. (2013). Introducing the UCDP georeferenced event dataset. *Journal of Peace Research*, *50*(4), 523–532. https://doi.org/10.1177/0022343313484347

Tangara, M. B. (2024). *The effects of armed conflicts on local economic dynamics in the Mopti and Ségou regions of Mali*. *The Economics of Peace and Security Journal, 19*(2), 35–54. https://doi.org/10.15355/epsj.19.2.35

Traoré, O. (2022, September 21). *Bandiagara : Entre insécurité et coupure d'électricité*. *Mali Actu*. https://maliactu.net/bandiagara-entre-insecurite-et-coupure-delectricite

United Nations. (2013). United Nations Multidimensional Integrated Stabilization Mission in Mali (MINUSMA). Retrieved from https://peacekeeping.un.org/en/mission/minusma

Wang, J., Ge, Y., & He, L. (2015). Rule-based land use/land cover classification in coastal areas using seasonal remote sensing imagery: A case study from Lianyungang City, China. *Marine Geodesy*, *45*(6), 633–654. https://doi.org/10.1080/01490419.2022.2085340

Weldegebriel, L., Negash, E., Nyssen, J., & Lobell, D. B. (2024). Eyes in the sky on Tigray, Ethiopia: Monitoring the impact of armed conflict on cultivated highlands using satellite imagery. *Science of Remote Sensing*, *9*, Article 100133. https://doi.org/10.1016/j.srs.2024.100133

Witmer, F. D. W., & O'Loughlin, J. (2011). Detecting the effects of wars in the Caucasus regions of Russia and Georgia using radiometrically normalized DMSP-OLS nighttime lights imagery. *GIScience & Remote Sensing*, *48*(4), 478–500. https://doi.org/10.2747/1548-1603.48.4.478

Xu, N., Zhuang, H., Chen, Y., Wu, S., & Liu, R. (2025). Mapping multi-crop cropland abandonment in conflict-affected Ukraine based on MODIS time series analysis. *Land*, *14*(8), Article 1548. https://doi.org/10.3390/land14081548

Yin, H., Butsic, V., Buchner, J., Kuemmerle, T., Prishchepov, A. V., Baumann, M., Bragina, E. V., Sayadyan, H., & Radeloff, V. C. (2019). Agricultural abandonment and re-cultivation during and after the Chechen Wars in the northern Caucasus. *Global Environmental Change*, *55*, 149–159. https://doi.org/10.1016/j.gloenvcha.2019.01.005

Yin, H., Brandão, A., Jr., Buchner, J., Helmers, D., Iuliano, B. G., Kimambo, N. E., Lewińska, K. E., Razenkova, E., Rizayeva, A., Rogova, N., Spawn, S. A., Xie, Yanhua, & Radeloff, V. C. (2020). Monitoring cropland abandonment with Landsat time series. *Remote Sensing of Environment*, *246*, Article 111873. https://doi.org/10.1016/j.rse.2020.111873

Zhang, Y., & Li, X. (2025). Assessment of Central Sahel crisis by nighttime light imagery. *IEEE Journal of Selected Topics in Applied Earth Observations and Remote Sensing, 18*, 13359–13371. https://doi.org/10.1109/JSTARS.2025.3570758

Appendix A: High resolution images showing built-up area expansion in Bandiagara.

Bandiagara 2016

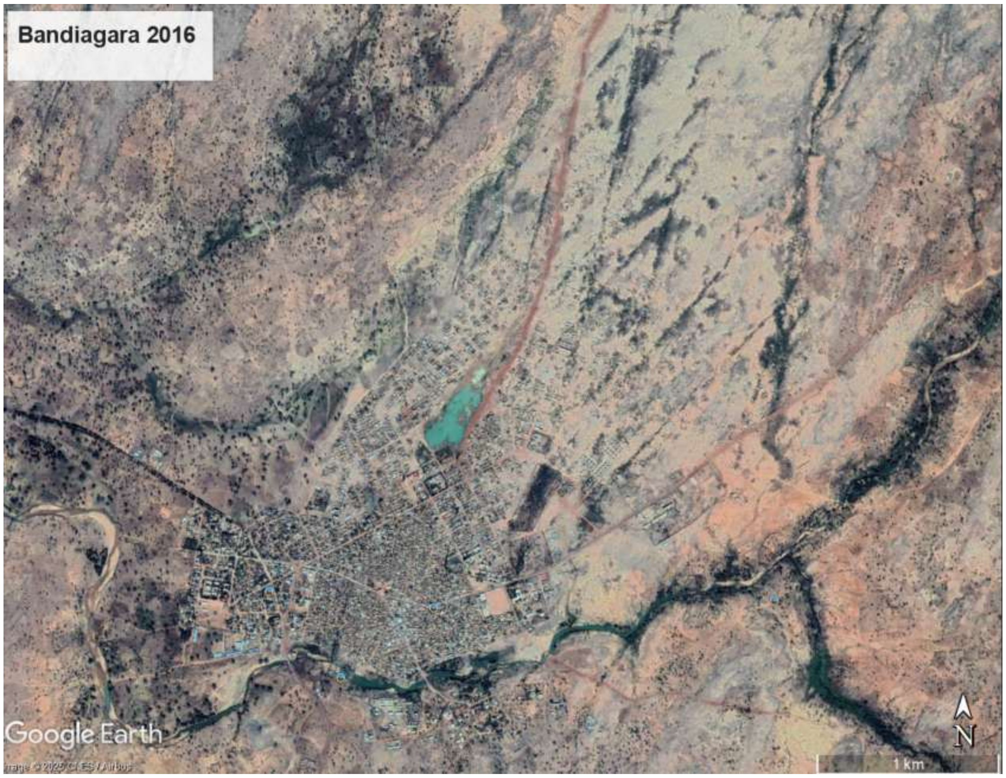

Bandiagara 2024

Appendix B: high resolution images showing total destruction of Bobosso settlement.

Bobosso Early 2019

Bobosso Early 2024

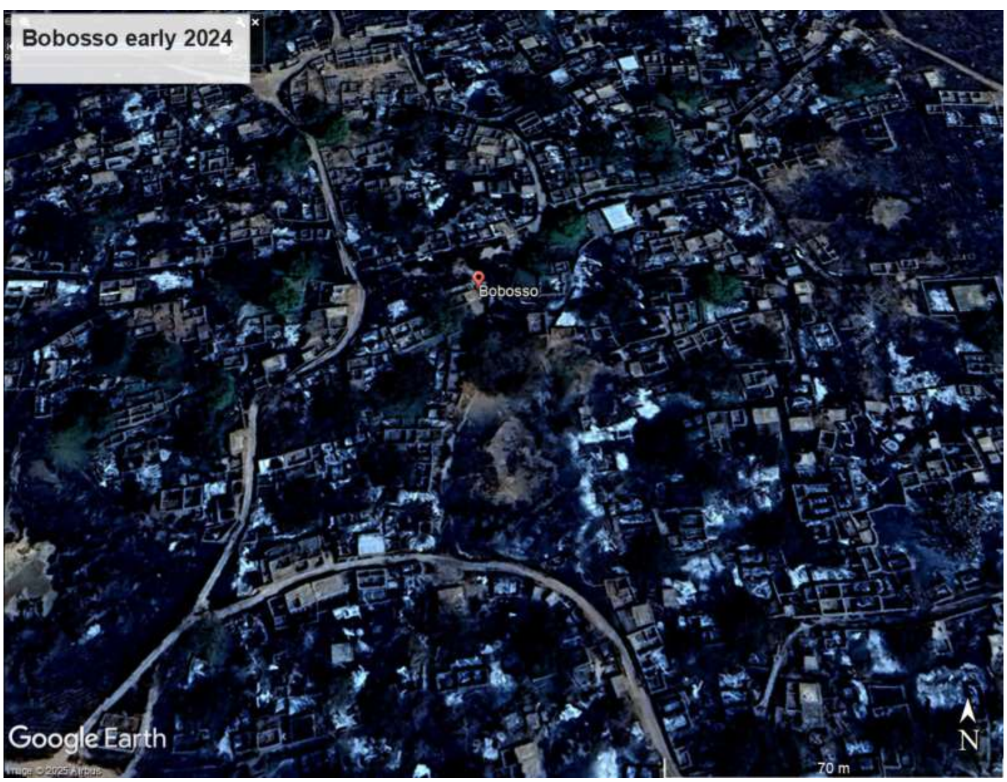

Appendix C: 3PTS script

```
// This script produces 3-period timescans for the years 2016 to 2023 in the Mopti region in Mali,
// in order to visually compare cropland areas and evaluate the impact of conflict on agriculture
// Credit : Adapted from Laure Boudinaud (WFP, Mali Country Office, VAM unit)

var point = ee.Geometry.Point(-2.93884, 14.93017);// _Douentza
var aoi = point.buffer(5e3);
Map.centerObject(aoi, 13);

// Create region
var region = point.buffer(15e3);

// Set time variables
var t1 = 166; // 15Jun
var t2 = 228;// 15Aug
var t3 = 259; // 15Sep
var t4 = 283; //10Oct

// CLOUD MASK FUNCTION
var maskS2_QA60 = function(image) {
        var qa = image.select('QA60');
        var cloudBitMask  = (1 << 10);
        var mask = qa.bitwiseAnd(cloudBitMask).eq(0)
        .and(qa.bitwiseAnd(cirrusBitMask).eq(0));
        return image.updateMask(mask);
        };

// Create a function to DONWLOAD the Sentinel-2 collection for a year of interest

var sentinel2 = function(year) {
        var start = year+''+'-01-01';
        var end = year+''+'-12-31';
        return ee.ImageCollection('COPERNICUS/S2')
        .filterDate(start, end)
        .filterBounds(aoi);

// Create a function to calculate and add NDVI band to the collection
var addNDVI = function(image) {
        var ndvi = image.normalizedDifference(['B8', 'B4']);
        return image.addBands(ndvi.rename('NDVI'));
        };

var s2016 = sentinel2(2016).map(addNDVI);
print('Sentinel collection 2016', s2016);
var s2017 = sentinel2(2017).map(addNDVI);
print('Sentinel collection 2017', s2017);
var s2018 = sentinel2(2018).map(addNDVI);
print('Sentinel collection 2018', s2018);
var s2019 = sentinel2(2019).map(addNDVI);
print('Sentinel collection 2019', s2019);
var s2020 = sentinel2(2020).map(addNDVI);
print('Sentinel collection 2020', s2020);
var s2021 = sentinel2(2021).map(addNDVI);
print('Sentinel collection 2021', s2021);
var s2022 = sentinel2(2022).map(addNDVI);
print('Sentinel collection 2022', s2022);
var s2023 = sentinel2(2023).map(addNDVI);
print('Sentinel collection 2023', s2023);
```

```
///// 3-PERIODS TIMESCAN PRODUCTS /////

// 2017
// Visualize RGB from max-NDVI values in three distinct periods of the agricultural season

var p1 = s2017.filter(ee.Filter.dayOfYear(t1, t2)).select('NDVI').max();
var p2 = s2017.filter(ee.Filter.dayOfYear(t2+1, t3)).select('NDVI').max();
var p3 = s2017.filter(ee.Filter.dayOfYear(t3+1, t4)).select('NDVI').max();


//get min and max values in the aoi (for vizualisation)
var min_values = p2.reduceRegion('min', aoi, 100).values().getInfo();
var max_values = p2.reduceRegion('max', aoi, 100).values().getInfo();
var index_viz = {min: min_values, max: max_values};



// Stack the created rasters into one 3-band image
var stack_2017 = p1.addBands(p2).addBands(p3);

// Add the layer on the map (R, G, B) = (maxNDVI(t1, t2), maxNDVI(t2 + 1, t3), maxNDVI(t3 + 1, t4))
Map.addLayer(stack_2017.clip(region), index_viz, '2017'); // clip to cut it so specified region!!!



// Do the same for 2016
var p1_2016 = s2016.filter(ee.Filter.dayOfYear(t1, t2)).select('NDVI').max();
var p2_2016 = s2016.filter(ee.Filter.dayOfYear(t2+1, t3)).select('NDVI').max();
var p3_2016 = s2016.filter(ee.Filter.dayOfYear(t3+1, t4)).select('NDVI').max();
var p4_2016 = s2016.filter(ee.Filter.dayOfYear(t1, t2)).select('NDVI').min();
var p5_2016 = s2016.filter(ee.Filter.dayOfYear(t2+1, t3)).select('NDVI').min();
var p6_2016 = s2016.filter(ee.Filter.dayOfYear(t3+1, t4)).select('NDVI').min();
var stack_2016 =
p1_2016.addBands(p2_2016).addBands(p3_2016).addBands(p4_2016).addBands(p5_2016).addBands(p6_2016)
;
Map.addLayer(stack_2016.clip(region), index_viz, '2016', false);

// Do the same for 2018
var p1_2018 = s2018.filter(ee.Filter.dayOfYear(t1, t2)).select('NDVI').max();
var p2_2018 = s2018.filter(ee.Filter.dayOfYear(t2+1, t3)).select('NDVI').max();
var p3_2018 = s2018.filter(ee.Filter.dayOfYear(t3+1, t4)).select('NDVI').max();
var stack_2018 = p1_2018.addBands(p2_2018).addBands(p3_2018);
Map.addLayer(stack_2018.clip(region), index_viz, '2018', false); // re-use visualization min, max values used for
2017

// Do the same for 2019
var p1_2019 = s2019.filter(ee.Filter.dayOfYear(t1, t2)).select('NDVI').max();
var p2_2019 = s2019.filter(ee.Filter.dayOfYear(t2+1, t3)).select('NDVI').max();
var p3_2019 = s2019.filter(ee.Filter.dayOfYear(t3+1, t4)).select('NDVI').max();
var p4_2019 = s2019.filter(ee.Filter.dayOfYear(t1, t2)).select('NDVI').min();
var p5_2019 = s2019.filter(ee.Filter.dayOfYear(t2+1, t3)).select('NDVI').min();
var p6_2019 = s2019.filter(ee.Filter.dayOfYear(t3+1, t4)).select('NDVI').min();
var stack_2019 =
p1_2019.addBands(p2_2019).addBands(p3_2019).addBands(p4_2019).addBands(p5_2019).addBands(p6_2019)
;
Map.addLayer(stack_2019.clip(region), index_viz, '2019');
```

```
// Do the same for 2020
var p1_2020 = s2020.filter(ee.Filter.dayOfYear(t1, t2)).select('NDVI').max();
var p2_2020 = s2020.filter(ee.Filter.dayOfYear(t2+1, t3)).select('NDVI').max();
var p3_2020 = s2020.filter(ee.Filter.dayOfYear(t3+1, t4)).select('NDVI').max();
var stack_2020 = p1_2020.addBands(p2_2020).addBands(p3_2020);
Map.addLayer(stack_2020.clip(region), index_viz, '2020');

// Do the same for 2021
var p1_2021 = s2021.filter(ee.Filter.dayOfYear(t1, t2)).select('NDVI').max();
var p2_2021 = s2021.filter(ee.Filter.dayOfYear(t2+1, t3)).select('NDVI').max();
var p3_2021 = s2021.filter(ee.Filter.dayOfYear(t3+1, t4)).select('NDVI').max();
var stack_2021 = p1_2021.addBands(p2_2021).addBands(p3_2021);
Map.addLayer(stack_2021.clip(region), index_viz, '2021');

// Do the same for 2022
var p1_2022 = s2022.filter(ee.Filter.dayOfYear(t1, t2)).select('NDVI').max();
var p2_2022 = s2022.filter(ee.Filter.dayOfYear(t2+1, t3)).select('NDVI').max();
var p3_2022 = s2022.filter(ee.Filter.dayOfYear(t3+1, t4)).select('NDVI').max();
var stack_2022 = p1_2022.addBands(p2_2022).addBands(p3_2022);
Map.addLayer(stack_2022.clip(region), index_viz, '2022');

// Do the same for 2023
var p1_2023 = s2023.filter(ee.Filter.dayOfYear(t1, t2)).select('NDVI').max();
var p2_2023 = s2023.filter(ee.Filter.dayOfYear(t2+1, t3)).select('NDVI').max();
var p3_2023 = s2023.filter(ee.Filter.dayOfYear(t3+1, t4)).select('NDVI').max();
var stack_2023 = p1_2023.addBands(p2_2023).addBands(p3_2023);
Map.addLayer(stack_2023.clip(region), index_viz, '2023');

// Export the image, specifying the CRS, transform, and region (still to add - projection - scale reduced to 30 due
to size but needed at 10).
Export.image.toDrive({
        image: stack_2016, //laag met 3 perioden in RGB
        description: 'composite_2016',
        scale: 10,
        region: region
        });

Export.image.toDrive({
        image: stack_2017, //laag met 3 perioden in RGB
       description: 'composite_2017',
       scale: 10,
       region: region
       });

Export.image.toDrive({
      image: stack_2018, //laag met 3 perioden in RGB
      description: 'composite_2018',
      scale: 10,
      region: region
      });

Export.image.toDrive({
      image: stack_2019, //laag met 3 perioden in RGB
      description: 'composite_2019',
      scale: 10,
      region: region
      });
```

```
Export.image.toDrive({
	image: stack_2020, //laag met 3 perioden in RGB
	description: 'composite_2020',
	scale: 10,
	region: region
	});

Export.image.toDrive({
	image: stack_2021, //laag met 3 perioden in RGB
	description: 'composite_2021',
	scale: 10,
	region: region
	});

Export.image.toDrive({
	image: stack_2022, //laag met 3 perioden in RGB
	description: 'composite_2022',
	scale: 10,
	region: region
	});

Export.image.toDrive({
	image: stack_2023, //laag met 3 perioden in RGB
	description: 'composite_2023',
	scale: 10,
	region: region
	});
```

Department of Physical Geography and Ecosystem Science

Master Thesis in Geographical Information Science

1. *Anthony Lawther:* The application of GIS-based binary logistic regression for slope failure susceptibility mapping in the Western Grampian Mountains, Scotland (2008).
2. *Rickard Hansen:* Daily mobility in Grenoble Metropolitan Region, France. Applied GIS methods in time geographical research (2008).
3. *Emil Bayramov:* Environmental monitoring of bio-restoration activities using GIS and Remote Sensing (2009).
4. *Rafael Villarreal Pacheco:* Applications of Geographic Information Systems as an analytical and visualization tool for mass real estate valuation: a case study of Fontibon District, Bogota, Columbia (2009).
5. *Siri Oestreich Waage:* a case study of route solving for oversized transport: The use of GIS functionalities in transport of transformers, as part of maintaining a reliable power infrastructure (2010).
6. *Edgar Pimiento:* Shallow landslide susceptibility – Modelling and validation (2010).
7. *Martina Schäfer:* Near real-time mapping of floodwater mosquito breeding sites using aerial photographs (2010).
8. *August Pieter van Waarden-Nagel:* Land use evaluation to assess the outcome of the programme of rehabilitation measures for the river Rhine in the Netherlands (2010).
9. *Samira Muhammad:* Development and implementation of air quality data mart for Ontario, Canada: A case study of air quality in Ontario using OLAP tool. (2010).
10. *Fredros Oketch Okumu*: Using remotely sensed data to explore spatial and temporal relationships between photosynthetic productivity of vegetation and malaria transmission intensities in selected parts of Africa (2011).
11. *Svajunas Plunge:* Advanced decision support methods for solving diffuse water pollution problems (2011).
12. *Jonathan Higgins:* Monitoring urban growth in greater Lagos: A case study using GIS to monitor the urban growth of Lagos 1990 - 2008 and produce future growth prospects for the city (2011).
13. *Mårten Karlberg:* Mobile Map Client API: Design and Implementation for Android (2011).
14. *Jeanette McBride:* Mapping Chicago area urban tree canopy using color infrared imagery (2011).

15. *Andrew Farina:* Exploring the relationship between land surface temperature and vegetation abundance for urban heat island mitigation in Seville, Spain (2011).

16. *David Kanyari*: Nairobi City Journey Planner: An online and a Mobile Application (2011).

17. *Laura V. Drews:* Multi-criteria GIS analysis for siting of small wind power plants - A case study from Berlin (2012).

18. *Qaisar Nadeem:* Best living neighborhood in the city - A GIS based multi criteria evaluation of ArRiyadh City (2012).

19. *Ahmed Mohamed El Saeid Mustafa:* Development of a photo voltaic building rooftop integration analysis tool for GIS for Dokki District, Cairo, Egypt (2012).

20. *Daniel Patrick Taylor*: Eastern Oyster Aquaculture: Estuarine Remediation via Site Suitability and Spatially Explicit Carrying Capacity Modeling in Virginia's Chesapeake Bay (2013).

21. *Angeleta Oveta Wilson:* A Participatory GIS approach to *unearthing* Manchester's Cultural Heritage '*gold mine'* (2013).

22. *Ola Svensson:* Visibility and Tholos Tombs in the Messenian Landscape: A Comparative Case Study of the Pylian Hinterlands and the Soulima Valley (2013).

23. *Monika Ogden:* Land use impact on water quality in two river systems in South Africa (2013).

24. *Stefan Rova:* A GIS based approach assessing phosphorus load impact on Lake Flaten in Salem, Sweden (2013).

25. *Yann Buhot:* Analysis of the history of landscape changes over a period of 200 years. How can we predict past landscape pattern scenario and the impact on habitat diversity? (2013).

26. *Christina Fotiou:* Evaluating habitat suitability and spectral heterogeneity models to predict weed species presence (2014).

27. *Inese Linuza:* Accuracy Assessment in Glacier Change Analysis (2014).

28. *Agnieszka Griffin:* Domestic energy consumption and social living standards: a GIS analysis within the Greater London Authority area (2014).

29. *Brynja Guðmundsdóttir:* Detection of potential arable land with remote sensing and GIS - A Case Study for Kjósarhreppur (2014).

30. *Oleksandr Nekrasov:* Processing of MODIS Vegetation Indices for analysis of agricultural droughts in the southern Ukraine between the years 2000-2012 (2014).

31. *Sarah Tressel:* Recommendations for a polar Earth science portal in the context of Arctic Spatial Data Infrastructure (2014).

32. *Caroline Gevaert:* Combining Hyperspectral UAV and Multispectral Formosat-2 Imagery for Precision Agriculture Applications (2014).

33. *Salem Jamal-Uddeen:* Using GeoTools to implement the multi-criteria evaluation analysis - weighted linear combination model (2014).

34. *Samanah Seyedi-Shandiz:* Schematic representation of geographical railway network at the Swedish Transport Administration (2014).

35. *Kazi Masel Ullah:* Urban Land-use planning using Geographical Information System and analytical hierarchy process: case study Dhaka City (2014).

36. *Alexia Chang-Wailing Spitteler:* Development of a web application based on MCDA and GIS for the decision support of river and floodplain rehabilitation projects (2014).

37. *Alessandro De Martino:* Geographic accessibility analysis and evaluation of potential changes to the public transportation system in the City of Milan (2014).

38. *Alireza Mollasalehi:* GIS Based Modelling for Fuel Reduction Using Controlled Burn in Australia. Case Study: Logan City, QLD (2015).

39. *Negin A. Sanati:* Chronic Kidney Disease Mortality in Costa Rica; Geographical Distribution, Spatial Analysis and Non-traditional Risk Factors (2015).

40. *Karen McIntyre:* Benthic mapping of the Bluefields Bay fish sanctuary, Jamaica (2015).

41. *Kees van Duijvendijk:* Feasibility of a low-cost weather sensor network for agricultural purposes: A preliminary assessment (2015).

42. *Sebastian Andersson Hylander:* Evaluation of cultural ecosystem services using GIS (2015).

43. *Deborah Bowyer:* Measuring Urban Growth, Urban Form and Accessibility as Indicators of Urban Sprawl in Hamilton, New Zealand (2015).

44. *Stefan Arvidsson:* Relationship between tree species composition and phenology extracted from satellite data in Swedish forests (2015).

45. *Damián Giménez Cruz*: GIS-based optimal localisation of beekeeping in rural Kenya (2016).

46. *Alejandra Narváez Vallejo:* Can the introduction of the topographic indices in LPJ-GUESS improve the spatial representation of environmental variables? (2016).

47. *Anna Lundgren:* Development of a method for mapping the highest coastline in Sweden using breaklines extracted from high resolution digital elevation models (2016).

48. *Oluwatomi Esther Adejoro:* Does location also matter? A spatial analysis of social achievements of young South Australians (2016).

49. *Hristo Dobrev Tomov:* Automated temporal NDVI analysis over the Middle East for the period 1982 - 2010 (2016).

50. *Vincent Muller:* Impact of Security Context on Mobile Clinic Activities A GIS Multi Criteria Evaluation based on an MSF Humanitarian Mission in Cameroon (2016).

51. *Gezahagn Negash Seboka:* Spatial Assessment of NDVI as an Indicator of Desertification in Ethiopia using Remote Sensing and GIS (2016).

52. *Holly Buhler:* Evaluation of Interfacility Medical Transport Journey Times in Southeastern British Columbia. (2016).

53. *Lars Ole Grottenberg*: Assessing the ability to share spatial data between emergency management organisations in the High North (2016).

54. *Sean Grant:* The Right Tree in the Right Place: Using GIS to Maximize the Net Benefits from Urban Forests (2016).

55. *Irshad Jamal:* Multi-Criteria GIS Analysis for School Site Selection in Gorno-Badakhshan Autonomous Oblast, Tajikistan (2016).

56. *Fulgencio Sanmartín:* Wisdom-volkano: A novel tool based on open GIS and time-series visualization to analyse and share volcanic data (2016).

57. *Nezha Acil:* Remote sensing-based monitoring of snow cover dynamics and its influence on vegetation growth in the Middle Atlas Mountains (2016).

58. *Julia Hjalmarsson:* A Weighty Issue: Estimation of Fire Size with Geographically Weighted Logistic Regression (2016).

59. *Mathewos Tamiru Amato:* Using multi-criteria evaluation and GIS for chronic food and nutrition insecurity indicators analysis in Ethiopia (2016).

60. *Karim Alaa El Din Mohamed Soliman El Attar:* Bicycling Suitability in Downtown, Cairo, Egypt (2016).

61. *Gilbert Akol Echelai:* Asset Management: Integrating GIS as a Decision Support Tool in Meter Management in National Water and Sewerage Corporation (2016).

62. *Terje Slinning:* Analytic comparison of multibeam echo soundings (2016).

63. *Gréta Hlín Sveinsdóttir:* GIS-based MCDA for decision support: A framework for wind farm siting in Iceland (2017).

64. *Jonas Sjögren:* Consequences of a flood in Kristianstad, Sweden: A GIS-based analysis of impacts on important societal functions (2017).

65. *Nadine Raska:* 3D geologic subsurface modelling within the Mackenzie Plain, Northwest Territories, Canada (2017).

66. *Panagiotis Symeonidis*: Study of spatial and temporal variation of atmospheric optical parameters and their relation with PM 2.5 concentration over Europe using GIS technologies (2017).

67. *Michaela Bobeck:* A GIS-based Multi-Criteria Decision Analysis of Wind Farm Site Suitability in New South Wales, Australia, from a Sustainable Development Perspective (2017).

68. *Raghdaa Eissa*: Developing a GIS Model for the Assessment of Outdoor Recreational Facilities in New Cities Case Study: Tenth of Ramadan City, Egypt (2017).

69. *Zahra Khais Shahid*: Biofuel plantations and isoprene emissions in Svea and Götaland (2017).

70. *Mirza Amir Liaquat Baig*: Using geographical information systems in epidemiology: Mapping and analyzing occurrence of diarrhea in urban - residential area of Islamabad, Pakistan (2017).

71. *Joakim Jörwall*: Quantitative model of Present and Future well-being in the EU-28: A spatial Multi-Criteria Evaluation of socioeconomic and climatic comfort factors (2017).

72. *Elin Haettner*: Energy Poverty in the Dublin Region: Modelling Geographies of Risk (2017).

73. *Harry Eriksson*: Geochemistry of stream plants and its statistical relations to soil- and bedrock geology, slope directions and till geochemistry. A GIS-analysis of small catchments in northern Sweden (2017).

74. *Daniel Gardevärn:* PPGIS and Public meetings – An evaluation of public participation methods for urban planning (2017).

75. *Kim Friberg:* Sensitivity Analysis and Calibration of Multi Energy Balance Land Surface Model Parameters (2017).

76. *Viktor Svanerud:* Taking the bus to the park? A study of accessibility to green areas in Gothenburg through different modes of transport (2017).

77. *Lisa-Gaye Greene*: Deadly Designs: The Impact of Road Design on Road Crash Patterns along Jamaica's North Coast Highway (2017).

78. *Katarina Jemec Parker*: Spatial and temporal analysis of fecal indicator bacteria concentrations in beach water in San Diego, California (2017).

79. *Angela Kabiru*: An Exploratory Study of Middle Stone Age and Later Stone Age Site Locations in Kenya's Central Rift Valley Using Landscape Analysis: A GIS Approach (2017).

80. *Kristean Björkmann*: Subjective Well-Being and Environment: A GIS-Based Analysis (2018).

81. *Williams Erhunmonmen Ojo*: Measuring spatial accessibility to healthcare for people living with HIV-AIDS in southern Nigeria (2018).

82. *Daniel Assefa*: Developing Data Extraction and Dynamic Data Visualization (Styling) Modules for Web GIS Risk Assessment System (WGRAS). (2018).

83. *Adela Nistora*: Inundation scenarios in a changing climate: assessing potential impacts of sea-level rise on the coast of South-East England (2018).

84. *Marc Seliger*: Thirsty landscapes - Investigating growing irrigation water consumption and potential conservation measures within Utah's largest master-planned community: Daybreak (2018).

85. *Luka Jovičić*: Spatial Data Harmonisation in Regional Context in Accordance with INSPIRE Implementing Rules (2018).

86. *Christina Kourdounouli*: Analysis of Urban Ecosystem Condition Indicators for the Large Urban Zones and City Cores in EU (2018).

87. *Jeremy Azzopardi*: Effect of distance measures and feature representations on distance-based accessibility measures (2018).

88. *Patrick Kabatha*: An open source web GIS tool for analysis and visualization of elephant GPS telemetry data, alongside environmental and anthropogenic variables (2018).

89. *Richard Alphonce Giliba*: Effects of Climate Change on Potential Geographical Distribution of Prunus africana (African cherry) in the Eastern Arc Mountain Forests of Tanzania (2018).

90. *Eiður Kristinn Eiðsson*: Transformation and linking of authoritative multi-scale geodata for the Semantic Web: A case study of Swedish national building data sets (2018).

91. *Niamh Harty*: HOP!: a PGIS and citizen science approach to monitoring the condition of upland paths (2018).

92. *José Estuardo Jara Alvear*: Solar photovoltaic potential to complement hydropower in Ecuador: A GIS-based framework of analysis (2018).

93. *Brendan O'Neill*: Multicriteria Site Suitability for Algal Biofuel Production Facilities (2018).

94. *Roman Spataru*: Spatial-temporal GIS analysis in public health – a case study of polio disease (2018).

95. *Alicja Miodońska*: Assessing evolution of ice caps in Suðurland, Iceland, in years 1986 - 2014, using multispectral satellite imagery (2019).

96. *Dennis Lindell Schettini*: A Spatial Analysis of Homicide Crime's Distribution and Association with Deprivation in Stockholm Between 2010-2017 (2019).

97. *Damiano Vesentini*: The Po Delta Biosphere Reserve: Management challenges and priorities deriving from anthropogenic pressure and sea level rise (2019).

98. *Emilie Arnesten*: Impacts of future sea level rise and high water on roads, railways and environmental objects: a GIS analysis of the potential effects of increasing sea levels and highest projected high water in Scania, Sweden (2019).

99. *Syed Muhammad Amir Raza*: Comparison of geospatial support in RDF stores: Evaluation for ICOS Carbon Portal metadata (2019).

100. *Hemin Tofiq*: Investigating the accuracy of Digital Elevation Models from UAV images in areas with low contrast: A sandy beach as a case study (2019).

101. *Evangelos Vafeiadis*: Exploring the distribution of accessibility by public transport using spatial analysis. A case study for retail concentrations and public hospitals in Athens (2019).

102. *Milan Sekulic*: Multi-Criteria GIS modelling for optimal alignment of roadway by-passes in the Tlokweng Planning Area, Botswana (2019).

103. *Ingrid Piirisaar*: A multi-criteria GIS analysis for siting of utility-scale photovoltaic solar plants in county Kilkenny, Ireland (2019).

104. *Nigel Fox*: Plant phenology and climate change: possible effect on the onset of various wild plant species' first flowering day in the UK (2019).

105. *Gunnar Hesch*: Linking conflict events and cropland development in Afghanistan, 2001 to 2011, using MODIS land cover data and Uppsala Conflict Data Programme (2019).

106. *Elijah Njoku*: Analysis of spatial-temporal pattern of Land Surface Temperature (LST) due to NDVI and elevation in Ilorin, Nigeria (2019).

107. *Katalin Bunyevácz*: Development of a GIS methodology to evaluate informal urban green areas for inclusion in a community governance program (2019).

108. *Paul dos Santos*: Automating synthetic trip data generation for an agent-based simulation of urban mobility (2019).

109. *Robert O' Dwyer*: Land cover changes in Southern Sweden from the mid-Holocene to present day: Insights for ecosystem service assessments (2019).

110. *Daniel Klingmyr*: Global scale patterns and trends in tropospheric NO2 concentrations (2019).

111. *Marwa Farouk Elkabbany*: Sea Level Rise Vulnerability Assessment for Abu Dhabi, United Arab Emirates (2019).

112. *Jip Jan van Zoonen*: Aspects of Error Quantification and Evaluation in Digital Elevation Models for Glacier Surfaces (2020).

113. *Georgios Efthymiou*: The use of bicycles in a mid-sized city – benefits and obstacles identified using a questionnaire and GIS (2020).

114. *Haruna Olayiwola Jimoh*: Assessment of Urban Sprawl in MOWE/IBAFO Axis of Ogun State using GIS Capabilities (2020).

115. *Nikolaos Barmpas Zachariadis*: Development of an iOS, Augmented Reality for disaster management (2020).

116. *Ida Storm*: ICOS Atmospheric Stations: Spatial Characterization of CO2 Footprint Areas and Evaluating the Uncertainties of Modelled CO2 Concentrations (2020).

117. *Alon Zuta*: Evaluation of water stress mapping methods in vineyards using airborne thermal imaging (2020).

118. *Marcus Eriksson*: Evaluating structural landscape development in the municipality Upplands-Bro, using landscape metrics indices (2020).

119. *Ane Rahbek Vierø*: Connectivity for Cyclists? A Network Analysis of Copenhagen's Bike Lanes (2020).

120. *Cecilia Baggini*: Changes in habitat suitability for three declining Anatidae species in saltmarshes on the Mersey estuary, North-West England (2020).

121. *Bakrad Balabanian*: Transportation and Its Effect on Student Performance (2020).

122. *Ali Al Farid*: Knowledge and Data Driven Approaches for Hydrocarbon Microseepage Characterizations: An Application of Satellite Remote Sensing (2020).

123. *Bartlomiej Kolodziejczyk*: Distribution Modelling of Gene Drive-Modified Mosquitoes and Their Effects on Wild Populations (2020).

124. *Alexis Cazorla*: Decreasing organic nitrogen concentrations in European water bodies - links to organic carbon trends and land cover (2020).

125. *Kharid Mwakoba*: Remote sensing analysis of land cover/use conditions of community-based wildlife conservation areas in Tanzania (2021).

126. *Chinatsu Endo*: Remote Sensing Based Pre-Season Yellow Rust Early Warning in Oromia, Ethiopia (2021).

127. *Berit Mohr*: Using remote sensing and land abandonment as a proxy for long-term human out-migration. A Case Study: Al-Hassakeh Governorate, Syria (2021).

128. *Kanchana Nirmali Bandaranayake*: Considering future precipitation in delineation locations for water storage systems - Case study Sri Lanka (2021).

129. *Emma Bylund*: Dynamics of net primary production and food availability in the aftermath of the 2004 and 2007 desert locust outbreaks in Niger and Yemen (2021).

130. *Shawn Pace*: Urban infrastructure inundation risk from permanent sea-level rise scenarios in London (UK), Bangkok (Thailand) and Mumbai (India): A comparative analysis (2021).

131. *Oskar Evert Johansson*: The hydrodynamic impacts of Estuarine Oyster reefs, and the application of drone technology to this study (2021).

132. *Pritam Kumarsingh*: A Case Study to develop and test GIS/SDSS methods to assess the production capacity of a Cocoa Site in Trinidad and Tobago (2021).

133. *Muhammad Imran Khan*: Property Tax Mapping and Assessment using GIS (2021).

134. *Domna Kanari*: Mining geosocial data from Flickr to explore tourism patterns: The case study of Athens (2021).

135. *Mona Tykesson Klubien*: Livestock-MRSA in Danish pig farms (2021).

136. *Ove Njøten*: Comparing radar satellites. Use of Sentinel-1 leads to an increase in oil spill alerts in Norwegian waters (2021).

137. *Panagiotis Patrinos*: Change of heating fuel consumption patterns produced by the economic crisis in Greece (2021).

138. *Lukasz Langowski*: Assessing the suitability of using Sentinel-1A SAR multi-temporal imagery to detect fallow periods between rice crops (2021).

139. *Jonas Tillman*: Perception accuracy and user acceptance of legend designs for opacity data mapping in GIS (2022).

140. *Gabriela Olekszyk*: ALS (Airborne LIDAR) accuracy: Can potential low data quality of ground points be modelled/detected? Case study of 2016 LIDAR capture over Auckland, New Zealand (2022).

141. *Luke Aspland*: Weights of Evidence Predictive Modelling in Archaeology (2022).

142. *Luís Fareleira Gomes*: The influence of climate, population density, tree species and land cover on fire pattern in mainland Portugal (2022).

143. *Andreas Eriksson*: Mapping Fire Salamander (Salamandra salamandra) Habitat Suitability in Baden-Württemberg with Multi-Temporal Sentinel-1 and Sentinel-2 Imagery (2022).

144. *Lisbet Hougaard Baklid*: Geographical expansion rate of a brown bear population in Fennoscandia and the factors explaining the directional variations (2022).

145. *Victoria Persson*: Mussels in deep water with climate change: Spatial distribution of mussel (Mytilus galloprovincialis) growth offshore in the French Mediterranean with respect to climate change scenario RCP 8.5 Long Term and Integrated Multi-Trophic Aquaculture (IMTA) using Dynamic Energy Budget (DEB) modelling (2022).

146. *Benjamin Bernard Fabien Gérard Borgeais*: Implementing a multi-criteria GIS analysis and predictive modelling to locate Upper Palaeolithic decorated caves in the Périgord noir, France (2022).

147. *Bernat Dorado-Guerrero*: Assessing the impact of post-fire restoration interventions using spectral vegetation indices: A case study in El Bruc, Spain (2022).

148. *Ignatius Gabriel Aloysius Maria Perera*: The Influence of Natural Radon Occurrence on the Severity of the COVID-19 Pandemic in Germany: A Spatial Analysis (2022).

149. *Mark Overton*: An Analysis of Spatially-enabled Mobile Decision Support Systems in a Collaborative Decision-Making Environment (2022).

150. *Viggo Lunde*: Analysing methods for visualizing time-series datasets in open-source web mapping (2022).

151. *Johan Viscarra Hansson*: Distribution Analysis of Impatiens glandulifera in Kronoberg County and a Pest Risk Map for Alvesta Municipality (2022).

152. *Vincenzo Poppiti*: GIS and Tourism: Developing strategies for new touristic flows after the Covid-19 pandemic (2022).

153. *Henrik Hagelin*: Wildfire growth modelling in Sweden - A suitability assessment of available data (2023).

154. *Gabriel Romeo Ferriols Pavico*: Where there is road, there is fire (influence): An exploratory study on the influence of roads in the spatial patterns of Swedish wildfires of 2018 (2023).

155. *Colin Robert Potter*: Using a GIS to enable an economic, land use and energy output comparison between small wind powered turbines and large-scale wind farms: the case of Oslo, Norway (2023).

156. *Krystyna Muszel*: Impact of Sea Surface Temperature and Salinity on Phytoplankton blooms phenology in the North Sea (2023).

157. *Tobias Rydlinge*: Urban tree canopy mapping - an open source deep learning approach (2023).

158. *Albert Wellendorf*: Multi-scale Bark Beetle Predictions Using Machine Learning (2023).

159. *Manolis Papadakis*: Use of Satellite Remote Sensing for Detecting Archaeological Features: An Example from Ancient Corinth, Greece (2023).

160. *Konstantinos Sourlamtas*: Developing a Geographical Information System for a water and sewer network, for monitoring, identification and leak repair - Case study: Municipal Water Company of Naoussa, Greece (2023).

161. *Xiaoming Wang*: Identification of restoration hotspots in landscape-scale green infrastructure planning based on model-predicted connectivity forest (2023).

162. *Sarah Sienaert*: Usability of Sentinel-1 C-band VV and VH SAR data for the detection of flooded oil palm (2023).

163. *Katarina Ekeroot*: Uncovering the spatial relationships between Covid-19 vaccine coverage and local politics in Sweden (2023).

164. *Nikolaos Kouskoulis*: Exploring patterns in risk factors for bark beetle attack during outbreaks triggered by drought stress with harvester data on attacked trees: A case study in Southeastern Sweden (2023).

165. *Jonas Almén*: Geographic polarization and clustering of partisan voting: A local-level analysis of Stockholm Municipality (2023).

166. *Sara Sharon Jones*: Tree species impact on Forest Fire Spread Susceptibility in Sweden (2023).

167. *Takura Matswetu*: Towards a Geographic Information Systems and Data-Driven Integration Management. Studying holistic integration through spatial accessibility of services in Tampere, Finland. (2023).

168. *Duncan Jones*: Investigating the influence of the tidal regime on harbour porpoise *Phocoena phocoena* distribution in Mount's Bay, Cornwall (2023).

169. *Jason Craig Joubert*: A comparison of remote sensed semi-arid grassland vegetation anomalies detected using MODIS and Sentinel-3, with anomalies in ground-based eddy covariance flux measurements (2023).

170. *Anastasia Sarelli*: Land cover classification using machine-learning techniques applied to fused multi-modal satellite imagery and time series data (2024).

171. *Athanasios Senteles*: Integrating Local Knowledge into the Spatial Analysis of Wind Power: The case study of Northern Tzoumerka, Greece (2024).

172. *Rebecca Borg:* Using GIS and satellite data to assess access of green area for children living in growing cities (2024).

173. *Panagiotis–Dimitrios Tsachageas*: Multicriteria Evaluation in Real Estate Land-use Suitability Analysis: The case of Volos, Greece (2024).

174. *Hugo Nilsson*: Inferring lane-level topology of signalised intersections from aerial imagery and OpenStreetMap using deep learning (2024).

175. *Pavlos Alexantonakis*: Estimating lake water volume fluctuations using Sentinel-2 and ICESat-2 remote sensing data (2024).

176. *Karl-Martin Wigen*: Physical barriers and where to find them (2024).

177. *Martin Storsnes*: Temporal RX-algorithm performance on Sentinel-2 images (2024).

178. *Saulė Gabrielė Petraitytė*: The Relation Between Covid-19 Vaccination and Voting Trends in Lithuania: A Spatial Analysis (2024).

179. *Pedro Martinez Duran*: Olive yield forecasting from remote sensing and climate datasets in the Jaen province (Spain) (2024).

180. *Josefine Kynde Hämberg*: Proximity to Urban Green Spaces for Older Adults in Specific Housings - a Case Study of Malmö, Sweden (2024).

181. *Max Bengtsson*: A Site Selection of An Energy Island in the North Sea: Optimal Location in an Ecological and an Economic Scenario Using a Multicriteria Decision Analysis (MCDA) (2024).

182. *Anna Börmann*: Assessing Great Britain as a relocation site for the threatened Iberian Lynx in a changing climate (2024).

183. *Josephine Roosli*: Flood Risk Assessment for the Kävlinge River for Present and Future Climate Scenarios using HEC-RAS Rain-on-Grid (2024).

184. *Seán Flanagan*: Spatiotemporal dynamics of E-scooter sharing ridership and their associations with the built environment: A Swedish comparative study (2024).

185. *Wouter Vorsters*: Assessing the Impact of Combined Sewer Overflow on the Habitat of Lampetra planeri: A Case Study in Flanders, Belgium (2025).

186. *Kathleen Macdonald*: Cetacean strandings on the Scottish coast: coastal accessibility factors lead to underreporting (2025).

187. *Athanasios Emmanouil Mourampetzis*: Navigating the Shadows: A Comparative Analysis of SAR and Optical Imagery for Detecting (Dark) Vessels (2025).

188. *Nizam-ud-Din*: Spatial Land Records System using Geospatial Techniques: a case study of a Mid-Sized Village in Pakistan (2025).

189. *Nedim Nasic Kjellgren*: Linked Geodata: Improving Rooftop Photovoltaic Production Estimates through BIM-GIS Integration using Semantic Web Technologies (2025).

190. *Vedrana Pretkovic*: Spatio-temporal vegetation changes in the Pacific-Chocó region of Colombia during the conflict and post-conflict periods (2025).

191. *Evelina Bengtsson*: A Socioeconomic Dimension of Crime: A Spatial Study of Firearm-related Violence in Malmö (2025).

192. *Martynas Bielinis*: Application of C-band Radar Interferometry for Dune Monitoring in the Curonian Spit (2025).

193. *Paulina Magdalena Rieke*: Case study of the benefits of BIM and GIS solutions used on a live infrastructure project (2025).

194. *Alina Schärer*: Evaluating the Impact of Urban Green Spaces and Vegetation Characteristics on Land Surface Temperature Across Swiss Cities Using Machine Learning (2025).

195. *Paul Stewart:* Where is wild in Glasgow's Southside? A test of the applicability of relative wildness mapping to suburban Scotland (2025).

196. *Georgios Fylakis:* Spatiotemporal analysis of the integration between shared e-scooters and public transport: Case studies in Oslo and Stockholm (2025).

197. *Andreas Klasson*: Generating 3D building models according to Swedish building specification using footprints and airborne laser scanning (2025).

198. *Agaton Järemo Lawin*: The spread of Japanese knotweed in Scania: Invasion suitability prediction using species distribution modelling (2025).

199. *Jesse Stewart:* Contextualizing the Geographic Influence on Infantry Manoeuvrability in a Historical Battlefield Using GIS: A Case Study of the Canadian Corps in the Second Battle of Passchendaele, First World War (2025).

200. *Oskar Vejkdal Thorsberg*: Automatic geometry extraction in digital building permits: A case study using BIM and NS Building (2025).

201. *Spyridon Gerafentis*: Impact of the COVID-19 "Lockdown" on Air Quality in Athens (2025).

202. *Symeon Andriotis*: Political Violence in Athens, Greece (2008-2024): A Machine Learning Approach for Predictive Modelling of Spatial Risk Patterns (2025).

203. *Simon Westman*: Detecting Structurally Old Scots Pine: A Crown-Metric Approach Using National ALS and LIFT Enrichment (2026).

204. *Freja Randeris Kristoffersen*: Satellite-Derived Bathymetry of Danish Coastal Waters Using Machine Learning with Sentinel-2 and ICESat-2 data (2026).

205. *Markus Honkanen*: Securitas Per Scientiam: GIS-MCDA of Civil Defence Shelter Distribution Efficiency in the Helsinki Capital Region (2026).

206. *Amanda Carolina Santos Motta*: Visualization Tools for Simulation Results Based on 3D City Models: An Urban Planner-Focused Study (2026).

207. *Gintars Krumins*: Mapping forest felling activities in Latvia from Sentinel-2 satellite imagery using machine learning (2026).

208. *Jenny Berntsson*: Using Multi-criteria GIS analysis in nature conservation planning in Lilla Edet municipality (2026).

209. *Sebastian Daland*: Flood impacts on road accessibility and buildings in Gothenburg during a 100-year rainfall event (2026).

210. *Polyxeni Karapanagiotidou*: GIS-based Multi-Criteria Decision Analysis (MCDA) framework for Flood Risk Assessment in the Thermi Basin (2026).

211. *Nour Abdulmagid A. Bensaid*: Urban Expansion and its Relation to the Urban Heat Island Effect: A Case Study of Tripoli, Libya (2026).

212. *Iris Krohn*: Compound Extreme Events in Hamburg, Germany: A Flood Risk Assessment (2026).

213. *Johan Wahlberg*: Towards Data-Centric Geospatial Applications: A Knowledge Graph Approach to Road Maintenance in Stockholm, Sweden (2026).

214. *Athanasios Fyntanidis*: Towards Data-Centric Geospatial Applications: Machine Learning–Driven Assessment of Urban Heat Island Intensity in Athens: Integrating Remote Sensing, Landscape Metrics, and Green Infrastructure for Climate-Resilient Urban Planning (2026).

215. *J.C.W. van Diest*: Detecting Spatial Impacts of Violence through Remote Sensing: A Case Study of Conflict-Affected Regions in Central Mali (2026).